WIMAX INNER RECEIVER DESIGN

By

ANG KEN LI

FINAL PROJECT REPORT

Submitted to the Electrical & Electronics Engineering Programme
in Partial Fulfilment of the Requirements
for the Degree
Bachelor of Engineering (Hons)
(Electrical & Electronics Engineering)

Universiti Teknologi Petronas
Bandar Seri Iskandar
31750 Tronoh
Perak Darul Ridzuan

CERTIFICATION OF APPROVAL

WIMAX INNER RECEIVER DESIGN

by

Ang Ken Li

A project dissertation submitted to the
Electrical & Electronics Engineering Programme
Universiti Teknologi PETRONAS
in partial fulfilment of the requirement for the
Bachelor of Engineering (Hons)
(Electrical & Electronics Engineering)
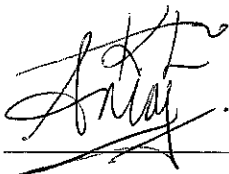
Approved:

_____
Assoc. Prof. Dr. Varun Jeoti
Project Supervisor

UNIVERSITI TEKNOLOGI PETRONAS

TRONOH, PERAK

June 2007

CERTIFICATION OF ORIGINALITY

This is to certify that I am responsible for the work submitted in this project, that the original work is my own except as specified in the references and acknowledgements, and that the original work contained herein have not been undertaken or done by unspecified sources or persons.

ANG KEN LI

ABSTRACT

"Igniting broadband wireless access". That is the vision for WiMAX, which is defined in the 802.16 standards to cover the frequency bands within the 2 to 66 GHz region. It promises an OFDM air interface with data rates comparable to wireline services (cable and xDSL). Coupled with QoS provisioning and support for NLOS propagation, WiMAX offers the platform for real time multimedia communications in addition to being able to replace the existing legacy PSTN. WiMAX also becomes the perfect launch pad for service providers to roll out triple play. The standard based products and availability of internet to anyone, anywhere and anytime will almost guarantee the widespread adoption of WiMAX everywhere.

This FYP attempts to simulate the working mechanism of a WiMAX receiver, with focus on synchronization (inner receiver), via simulation in Simulink. The undertaking will involve the baseband physical radio link. The proposed method of synchronization is a novel hybrid of a modified version of the Schmidl and Cox technique and the double sliding window packet detection. The inner receiver deals with synchronization issues such as FFT timing offset and carrier frequency offset. Offsets and impairments are deliberately introduced into the system to ensure that the receiver is totally blind and to fully test the proposed algorithm.

Results indicate that the proposed method can harness the best features of both worlds. Frame timing synchronization is achieved accurately without uncertainties of detecting a plateau. On the other hand, frequency offsets are dealt with efficiently using the tried and tested Schmidl and Cox technique. All in all, the proposed synchronization scheme is very well suited for WiMAX systems. The proposed method can achieve rapid synchronization with low overhead.

ACKNOWLEDGEMENTS

TABLE OF CONTENTS

LIST OF TABLES

LIST OF FIGURES

LIST OF ABBREVIATIONS

2G	Second Generation
3G	Third Generation
4G	Fourth Generation
ADC	Analogue to Digital Converter
AWGN	Additive White Gaussian Noise
B3G	Beyond 3rd Generation
BTS/BS	Base Station
BWA	Broadband Wireless Access
Cable TV	Cable Television
DC	Direct Current
FFT	Fast Fourier Transform
FIR	Finite Impulse Response
FPGA	Field Programmable Grid Array
GI	Guard Interval
GSM	Global System for Mobile communications
ICI	Inter Carrier Interference
IEEE	Institute of Electrical and Electronic Engineers
IF	Intermediate Frequency
IFFT	Inverse Fast Fourier Transform
IMT-2000	International Mobile Telecommunications in the year 2000
IPTV	Internet Protocol Television
IS-95	Interim Standard 95
ISI	Inter Symbol Interference
LAN	Local Area Network

LOS	Line of Sight
MAN	Metropolitan Area Network
NLOS	Non Line of Sight
OFDM	Orthogonal Frequency Division Multiplexing
PN	Pseudo-Noise
PSK	Phase Shift Keying
PSTN	Public Switched Telephone Network
QAM	Quadrature Amplitude Modulation
QoS	Quality of Service
RF	Radio Frequency
SC	Subcarrier
SNR	Signal to Noise Ratio
SUI	Stanford University Interim
TS	Training Symbol
UMTS	Universal Mobile Telecommunications System
VoIP	Voice over Internet Protocol
WAN	Wide Area Network
WiMAX	Worldwide Interoperability for Microwave Access
xDSL	x Digital Subscriber Line

CHAPTER 1

INTRODUCTION

Wireless communication has really taken off in the last decade with the emergence of 2nd Generations (2G) of digital cellular communications. A new chapter in the information and communication technology field was written with the worldwide successes of GSM and IS-95 systems. These systems were derived from a voice legacy, thus its primary services were all voice transmission. Nevertheless, there is a huge demand for ever increasing speeds for wireless multimedia services. With the advent of 3rd Generation (3G) wireless systems, it is expected that higher mobility with reasonable data rate (up to 2 Mbps) can be provided to meet the current user needs. But, 3G is not the end of the tunnel; ever increasing user demands have drawn the industry to search for better solutions to support data rates of the range of tens of Mbps.

1.1   Beyond 3rd Generation (B3G)

More and more service providers are joining the rat race to roll out "triple play" services to its customers. Hence, this convergence of voice, video and data will push the demand for high data rate to new heights. Given the vertical orientation of legacy systems like cable TV and PSTN, it is difficult and expensive to offer more than one type of service on any one "stovepipe" network [1].

"Third generation" (3G) cellular systems, called IMT-2000 and UMTS are currently deployed to meet this demand, supporting data rates up to 2 Mbps for local coverage and at least 144 kbps for wide-area coverage [2].
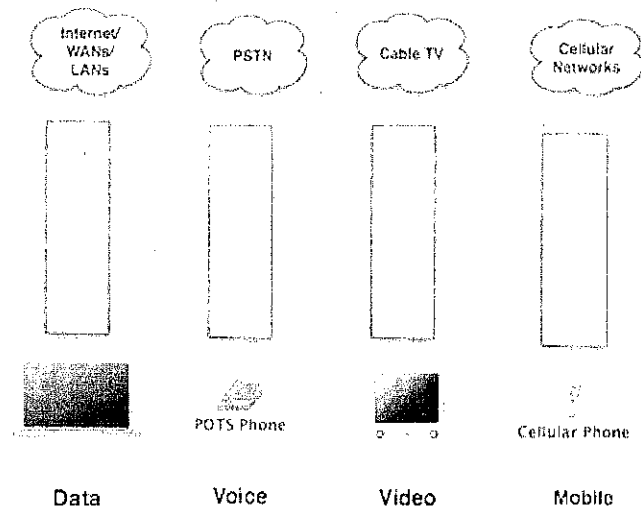
Figure 1   Legacy "stovepipe" infrastructure cannot easily offer more than one
service

While the roll out of 3G systems is under progress, research activities on the fourth generation (4G) have already started. WiMAX, defined as Worldwide Interoperability for Microwave Access, is envisioned as the 4th Generation system that can quench the current thirst for increasing speed. The WiMAX forum was formed in April 2001 to promote conformance and interoperability of the IEEE 802.16 [3] standard, also known as Wireless MAN.

1.2   WiMAX IEEE 802.16 – Igniting Broadband Wireless Access

WiMAX is defined in the IEEE 802.16 standard to cover frequency bands within the 2 to 66 GHz [3] region that will provide a wireless alternative to cable and xDSL level services for last mile broadband access, as well as providing backhaul for 801.11 hotspots [4]. The radio part of the IEEE 802.16 standard for WMAN is based on OFDM, a technique used to achieve data transmission in a bandwidth-efficient way.

It promises broadband connectivity without the need for LOS [5] and a single BTS (base station) shall suffice to serve up to hundreds of users. Moving on, this will serve as a launch pad for companies to build networks that permeate underserved business and residential markets that were previously left out due to geographical or

physical obstacles [4, 5]. The WiMAX standard also offers QoS provisioning and low latency access that can cater for a wide variety of applications.

POINT TO POINT for
connecting Base Stations
and feeding Cellular Towers

T1 LEVEL SERVICE for
SMEs

Internet
Backbone

Teleo Central
Office or Private
(Fiber) Network

DSL LEVEL SERVICE
for Small Business

WIRELESS BACKHAUL
for Hot Spots

RESIDENTIAL/SOHO
BROADBAND

Hot Spot
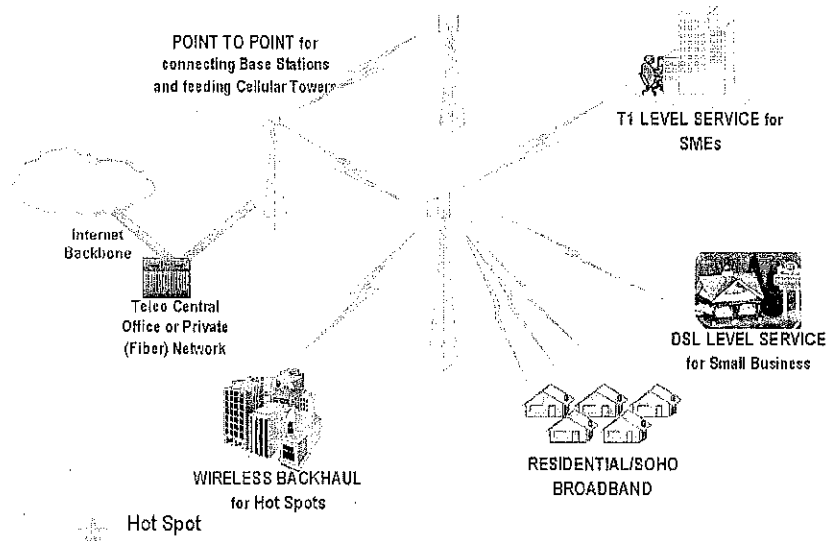
Figure 2   WiMAX topology – BWA everywhere

The most outstanding advantage of BWA is its low cost of installation and maintenance compared with traditional wireline or fiber network, especially for those areas that are too remote or difficult to reach [14]. BWA can extend fiber optic networks and provide more capacity than cable networks or DSL. Networks could be created in a short time by deploying a small number of BTS on buildings or poles to create high-capacity wireless access systems

A fixed wireless solution not only offers competitive internet access, it can do the same for telephone service thus further bypassing the telephone company's copper wire network. VoIP offers a wider range of voice services at reduced cost to subscribers and service providers alike. In fact, VoIP is seen as a "must have" in order for WiMAX to take off [6]. In addition, WiMAX will become an irresistible offer to consumers when bundled with IPTV [7], hence offering a complete "triple play" solution. Therefore, consumers can begin to experience exhilarating multimedia communications such as real time voice and video because QoS, security and

reliability are built into WiMAX [6]. Moreover, all WiMAX products are standard based which means that customers can purchase WiMAX equipment from any company and it will be compatible with other WiMAX certified products [4].

laptop | desk top PC
WiMAX as broadband internet access

TV or video monitor | TV or video monitor
WiMAX as cable or satellite TV bypass

WiMAX as landline telephone bypass

laptop
WiMAX as mobile data and cell phone bypass
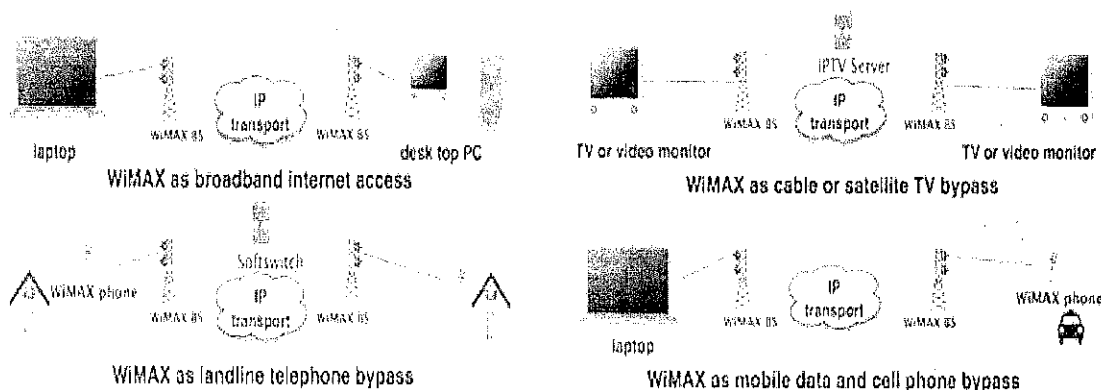
Figure 3   WiMAX has the potential to impact all forms of telecommunications

1.3   Problem Statement

The WiMAX air interface has to deal with ever unpredictable wireless channel for high data rate communications. Hostile wireless channel has always been proved to be a bottleneck for high speed wireless systems. This phenomenon shows the crucial requirement for accurate synchronization as a well-known problem of OFDM is its vulnerability to synchronization errors [8, 9, 10, 11, 12, 16].

In an OFDM system, synchronization at the receiver is one critical step that must be performed to ensure that the transmitted data symbols can be properly recovered. Synchronization of an OFDM signal requires finding the symbol timing and carrier frequency offset. Finding the symbol timing for OFDM means finding an estimate of where the symbol starts. On the other hand, synchronization of the carrier frequency at the receiver must be performed very accurately, or else there will be loss of orthogonality between the subsymbols.

9

1.4 Objective

This final year project undertaking attempts to design of a robust synchronization algorithm for WiMAX/OFDM systems. The said algorithm needs to be able to perform rapid synchronization with low overhead.

The first goal of this report is to create an overview of the area of OFDM synchronization. Several synchronization algorithms are studied and analyzed for their strengths and weaknesses. The aim of this endeavour would be to propose an algorithm that can harness the positive attributes of various systems.

The second goal will be to evaluate the performance of the proposed algorithm. A working simulation model conforming to the IEEE 802.16 standard and is able to achieve synchronization is expected.

1.5 Scope of Work

The following issues are analyzed and discussed in this dissertation:

- Modelling of an idealized WiMAX/OFDM system and the impact of small synchronization errors.

- Analysis of current synchronization algorithms.

- Design of a training symbol that is suited for synchronization but does not jeopardize channel estimation at the same time. The training symbol should consume the least possible resources.

- Development of a novel synchronization algorithm which is a hybrid that captures the strengths of various other methods.

- Modelling of the proposed algorithm and a complete simulation model.

- The work is focused on the physical layer baseband only.

1.6 Organization of this Final Report

This final report describes the work done in the WiMAX receiver design project. *Chapter 1* highlights WiMAX as an air interface capable of supplying high data rates. In addition, it describes how WiMAX can be the key enabling factor for "triple play". The significance of the synchronization task at the receiver and issues relating to it are listed in the *Problem Statement*. Next, the goal of simulating a working synchronization algorithm for WiMAX systems is outlined in the *Objective* while the *Scope of Work* section details the issues that are being investigated.

Chapter 2 Literature Review will give an insight into the OFDM theory that is the underlying technology behind WiMAX. Consequently, this will cover modulation, demodulation and the cyclic prefix. Next, an overview of the IEEE 802.16 standard is presented, highlighting the key parameters. After that, the synchronization errors involving FFT timing offset and carrier synchronization are explained.

Chapter 3 Methodology defines how the project will be implemented i.e. the receiver will be modelled and simulated in Simulink with appropriate offsets and impairments introduced into the system. Moving on, the conventional synchronization methods are analyzed before a description of the proposed algorithm.

This is followed by *Chapter 4 Results and Discussion* which depicts the various plots of decision metrics in addition to time domain signals before and after synchronization. Finally, several recommendations to further the work are given at the end of the report before the conclusion in *Chapter 5*.

CHAPTER 2
LITERATURE REVIEW

OFDM is a special case of multicarrier modulation [20] which leverages on parallel transmission. With this, it escapes the penalty of requiring heavy equalization [12, 15] in broadband communications as compared to single carrier systems. Nevertheless, it poses a stricter synchronization requirement compared to single carrier systems. This chapter delves into the OFDM theory and how cyclic prefix is used to combat ISI (inter symbol interference). Subsequently, an overview of the key OFDM parameters that make up the physical layer of WiMAX is presented. With that, a discussion about the effects of synchronization errors follows.

2.1 Motivation for Multicarrier Modulation

A single carrier system suffers from ISI problem when data rate is extremely high [19]. In the case of single carrier high speed wireless data transmission, the delay spread at such high data rate will definitely be greater than symbol duration even considering the best case outdoor scenario. This is due to the fact that the channel coherence bandwidth is much less than the bandwidth of the signal.

In a single carrier system, this situation is compensated by using adaptive equalization techniques [12, 18]. Adaptive equalization estimates the channel impulse response and multiplies complex conjugate of the estimated impulse response with the received data signal at the receiver. As ISI becomes more prevalent at high data rates, equalization becomes more complicated and complex. Nevertheless, there are some practical computational difficulties in performing these equalization techniques at tens of Mbps with compact and low cost hardware. Complex equalizers are very efficient in performance, but not cost efficient [19].

One way to achieve reasonable quality and also solve the problems described above for broadband communications is to use parallel transmission. This is where multicarrier modulation [20] comes into the picture. In a crude sense, multicarrier modulation is parallel transmission in principle. In essence, it is just the summation of a number of single carrier transmissions at the adjacent frequencies.

2.2 OFDM Basics

In OFDM, a subset of multicarrier modulation, the entire channel bandwidth is divided into several narrow sub-bands where each sub-band will experience flat fading. The flat fading condition is favoured in communication systems because it reduces the complex multi-tap equalizer in the frequency selective fading case to a simple one-tap equalizer [15]. A high data rate stream is divided it into several interleaved bit streams of lower data rate. These lower rate streams are then used to modulate several carriers simultaneously and are sent these over the many different sub-bands.
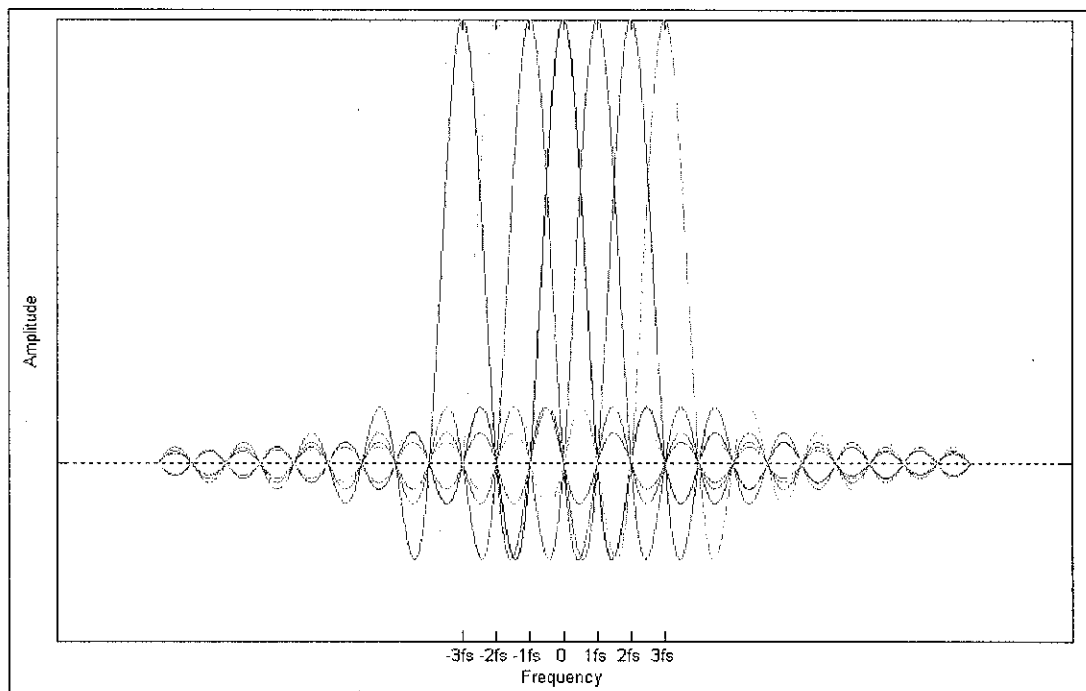
Figure 4   Spectrum of an OFDM signal

Each OFDM symbol contains subcarriers that are nonzero over a T-second interval. Hence, the spectrum of a single symbol is a convolution of a group of Dirac pulses located at subcarrier frequencies with the spectrum of a square pulse that is one for a T-second period and zero otherwise [9]. The amplitude spectrum of the square pulse is equal to sinc(πfT) which has zeroes for all frequencies f that are an integer multiple of $1/T$. The effect is shown in Figure 4, which shows the overlapping sinc spectra of individual subcarriers. At maximum of each subcarrier spectrum, all other subcarrier spectra are zero.

Because an OFDM receiver essentially calculates the spectrum values at those points that correspond to the maxima of individual subcarriers, it can demodulate any subcarrier free from any interference from other subcarriers. Basically, Figure 4 shows that the OFDM spectrum fulfils Nyquist criterion for an ISI free pulse shape. Consequently, instead of ISI, it is ICI that is avoided by having the maximum of one subcarrier correspond to the zero crossing of all the others [9].

The symbol duration of individual subcarriers is now longer than the original high data rate stream. As such the relative amount of time dispersion of an OFDM symbol in a normal multipath environment is significantly less than what would occur if the single stream of data were to be modulated by a single carrier [12, 18]. Hence, ISI is almost eliminated in this case. Moreover, a cyclic prefix is added to the OFDM symbols by repeating the tail of the symbol at the guard interval to eradicate ISI completely (*cf* Section 2.5).

2.3 OFDM System Model

An OFDM signal consists of a summation of subcarriers that are modulated by PSK or QAM. Mathematically, the complex baseband OFDM signal for the kth symbol can be expressed as follows

$$s_k(t - kT)$$

$$
= \begin{cases} w(t - kT) \displaystyle\sum_{i=-N/2}^{N/2-1} x_{i,k} e^{j2\pi\left[\frac{i}{T_{FFT}}\right](t-kT)} & kT - T_{win} - T_{guard} \leq t \leq kT + T_{FFT} + T_{win} \\ 0 & otherwise \end{cases}
$$

$$(2\text{-}1)$$

T	Symbol length; time between two consecutive OFDM symbols
T_{FFT}	FFT-time; effective part of the OFDM symbol
T_{guard}	Guard-interval; duration of the cyclic prefix
T_{win}	Window-interval; duration of windowed prefix/postfix for spectral shaping
f_c	Centre frequency of the occupied frequency spectrum
$F = 1/T_{FFT}$	frequency spacing between adjacent sub-carriers
N_{FFT}	length; number of FFT points
k	index on transmitted symbol
i	index on sub-carrier; $i \in \{-N/2, -N/2+1, \ldots, -1, 0, 1, \ldots, N/2-1\}$
$x_{i,k}$	signal constellation point; complex {data, pilot, null} symbol modulated on the i-th subcarrier of the k-th OFDM symbol

The window in the equation is of a raised cosine function. It has a value of 1 within T_{FFT} so it is not very significant in the modulation and demodulation process. The window is incorporated in order to reduce the level of side-lobes and therefore reduce the signal power transmitted out of band.

The effect of a time variant multipath channel can be modelled by a convolution with a channel impulse response of $h(t, \tau)$ and AWGN, $n(t)$. In this case $h(t, \tau)$.

$$
\begin{aligned}
r(t) &= h(\tau, t) * s(t) + n(t) \\
&= \int_{0}^{\tau_{max}} h(\tau, t) s(t - \tau) d\tau + n(t)
\end{aligned}
$$

$$(2\text{-}2)$$

15

Since a cyclic prefix (*cf* Section 2.5) is added to each OFDM symbol such that $T_{guard} \gg \tau_{max}$, no ISI occurs. This fact is illustrated in Figure 5 and Figure 6. With this, then the channel impulse response is simplified to $h(\tau)$ [9]. Consequently, the OFDM demodulation can be shown as follows [*s(t)* is defined earlier] :

$$
y_{i,k} = \frac{1}{T_{FFT}} \int_{i=kT}^{kT+T_{FFT}} r(t) e^{-j2\pi(t-kT)/T_{FFT}} dt
$$

$$
= \frac{1}{T_{FFT}} \int_{i=kT}^{kT+T_{FFT}} \left[\int_{\tau=0}^{\tau_{max}} h_k(\tau) s(t-\tau) d\tau + n(t) \right] e^{-j2\pi(t-kT)/T_{FFT}} dt
$$

$$
= \frac{1}{T_{FFT}} \int_{t=kT}^{kT+T_{FFT}} \left[\int_{\tau=0}^{\tau_{max}} h_k(\tau) \sum_{i'=-N/2}^{N/2-1} x_{i,k} e^{-j2\pi \left(\frac{i'}{T_{FFT}} \right)(t-kT-\tau)} d\tau \right] e^{-j2\pi(t-kT)/T_{FFT}} dt +
$$

$$
\frac{1}{T_{FFT}} \int_{i=kT}^{kT+T_{FFT}} n(t) e^{-j2\pi(t-kT)/T_{FFT}} dt
$$

(2-3)
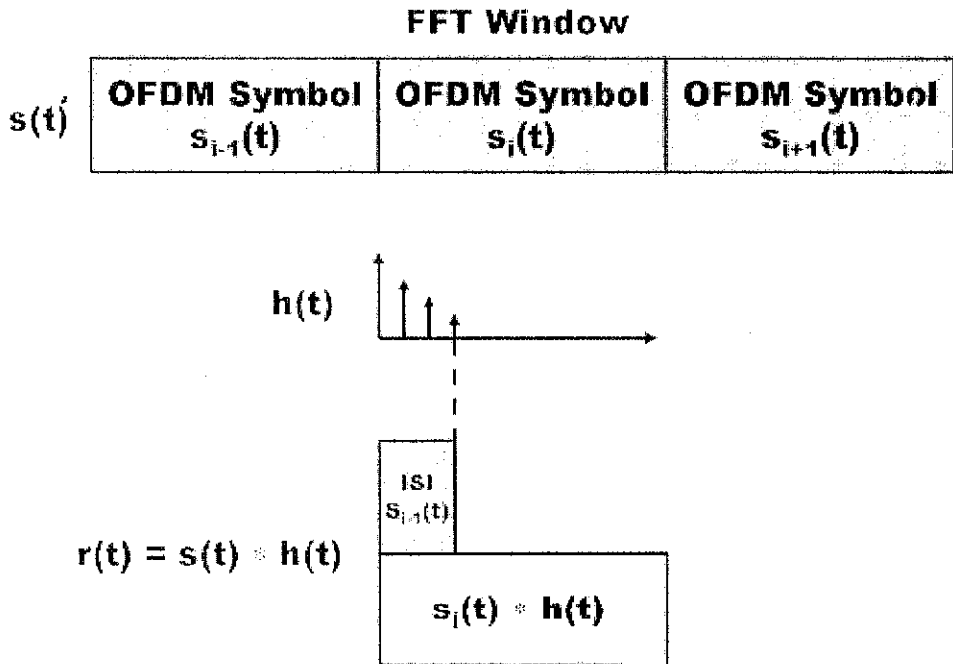
Figure 5   Channel induces ISI without cyclic prefix
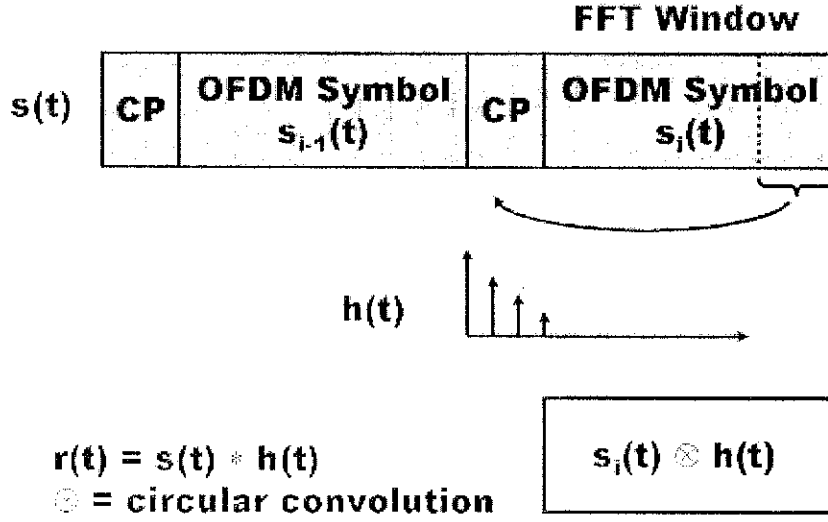
Figure 6   OFDM symbols with cyclic prefix prevents ISI

The second term represents independent AWGN and the integration of the $n(t)$ term yields $n_{i,k}$. Substituting $u = t - kT$, and changing the order of summation and integration yields:

$$y_{i,k} = \sum_{i'=-N/2}^{N/2-1} x_{i,k} \frac{1}{T_{FFT}} \int_{u=0}^{T_{FFT}} \left[\int_{\tau=0}^{\tau_{max}} h_k(\tau)e^{-j2\pi i'\tau/T_{FFT}} d\tau \right] e^{-j2\pi(i-i')u/T_{FFT}} du + n_{i,k}$$

$$(2\text{-}4)$$

The integration of the $h_k(\tau)$ term is actually the Fourier transform of the impulse response, which yields $h_{i,k}$. Noting this, the OFDM demodulation can then be resolved to:

$$y_{i,k} = \sum_{i'=-N/2}^{N/2-1} x_{i,k} h_{i,k} \frac{1}{T_{FFT}} \int_{u=0}^{T_{FFT}} e^{-j2\pi(i-i')u/T_{FFT}} du + n_{i,k}$$

$$y_{i,k} = x_{i,k} + n_{i,k}$$

$$(2\text{-}5)$$

The value of the integration will be 1 if and only if $i = i'$ and 0 otherwise. This also serves to demonstrate the orthogonal property. For $i \neq i'$, there are an integer number of sinusoids within T_{FFT} and the integration will become 0.

2.4 Guard Interval and Cyclic Prefix

In order to completely remove ISI in OFDM, a guard interval is integrated into each OFDM symbol. Its duration is selected such that it is larger than the maximum excess delay of the radio channel i.e the worst case scenario [8]. With this, the components of a particular symbol due to multipath will not interfere with the next symbol. Figure 7 shows how ISI is eliminated in OFDM by introducing a guard time. The delayed symbol 1 does not spill over to symbol 2 due to the guard time. Note that if the delay is longer than the guard time, ISI will also occur.
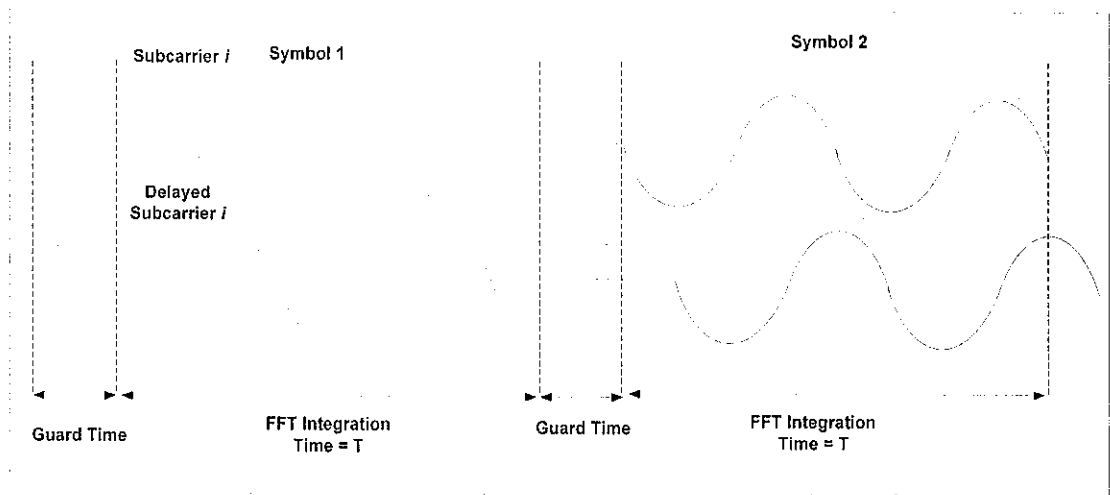
Figure 7   Effects of multipath with no signal within the guard interval

The guard interval may contain no signal at all as depicted in the following figure. In this case, ICI will ensue leading to a loss of orthogonality among subcarriers. With reference to figure 8, when the receiver tries to demodulate subcarrier i, it will encounter some interference from subcarrier j. This is because there is no longer integer multiples of cycle difference between subcarriers i and j during the FFT interval. Consequently, there will be crosstalk between subcarriers i and j for the same reason.
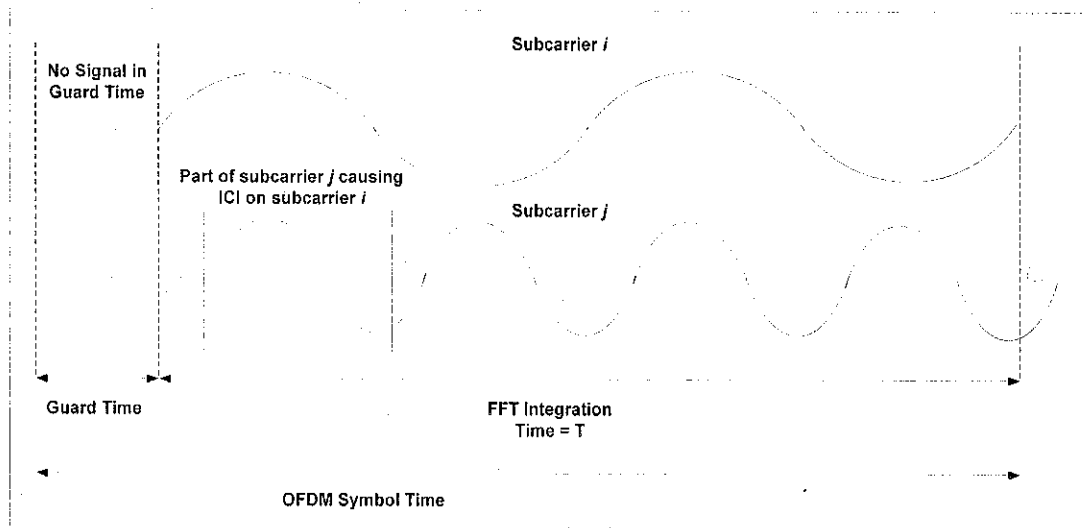
Figure 8 Effect of ICI in the absence of signal within the guard interval

In order to eliminate this ICI, the OFDM symbol is cyclically extended in the guard time (Figure 9). This ensures that the delayed replicas of the OFDM symbol always have an integer number of cycles within the FFT interval, as long as the delay spread is smaller than the guard time. Subsequently, the guard interval is also known as a cyclic prefix because a copy of the last part of the OFDM symbol is appended before the so-called "effective" part of the symbol. Therefore, the effective part of the received signal can be seen as the cyclic convolution of the transmitted OFDM symbol by the channel impulse response (cf Appendix A).
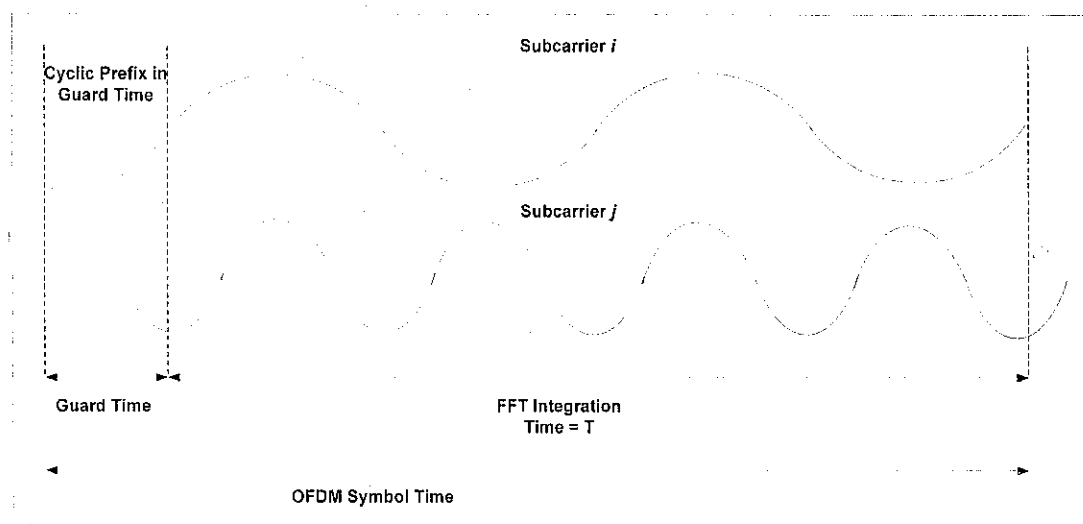
Figure 9 Elimination of ISI and ICI via cyclic prefix within the guard interval

2.5 Overview of WiMAX IEEE 802.16

The IEEE 802.16a standard specifies three air interfaces: single-carrier modulation, 256-point transform OFDM, and 2048-point transform OFDMA [3]. Nevertheless, mainstream implementations involve the 256 point FFT OFDM. By using 256 point FFT OFDM (compared with 64 point FFT in 802.11a), the symbol duration is prolonged and therefore it is very tolerant of the long multipath delays that occur in long-range, NLOS operation [14]. The following table lists key parameters for the WiMAX physical layer (mainstream implementation).

Table 1   256-OFDM WiMAX physical layer parameters [14]

| Parameters	Value
N_{FFT} : number of FFT/IFFT points	256
N_{used} : number of used carriers	200
F_s/BW :sampling frequency to bandwidth ratio	8/7 for license-exempt bands
T_g/T_b : Cyclic prefix lengths	1/4,1/8,1/16,1/32
Number of lower frequency guard carriers	28
Number of higher frequency guard carriers	27
Frequency offset indices of guard carriers	-128,-127...,-101 +101,+102,...+127
Frequency offset indices of basic fixed location of guard carriers	-84,-60,-36,-12,12,36,60,84
Channel bandwidth	20 MHz

The radio transmission takes place in a 20 MHz wide frequency band divided into 256 sub-bands. 200 of these sub-bands are used for actual data transmission. The standard also specifies variable cycle prefix lengths for different channel conditions to overcome different delay spreads. This is to maximize efficiency in low delay spread channels. The purpose of the guard carriers is to enable the signal to decay and create the FFT 'brick wall' shaping.

2.6 OFDM System Impairments

OFDM is highly sensitive to time and frequency synchronization errors, especially with frequency synchronization errors, everything can go wrong [21]. Demodulation of an OFDM signal with an offset in the frequency can lead to a high bit error rate. As an introduction to the work on synchronization algorithms, the relevant effects of synchronization errors are reviewed in this section. The following chart summarizes the synchronization errors and its sources.
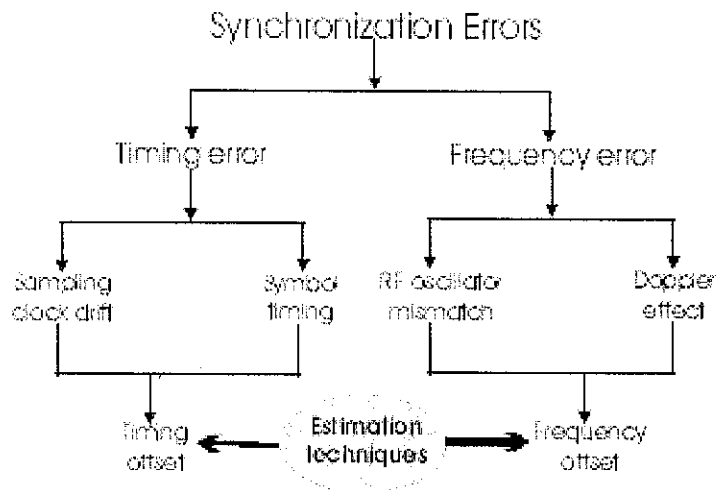
Figure 10   Synchronization errors in OFDM systems

2.6.1   FFT Time Synchronization Error

FFT time synchronization, frame detection and time offset estimation will be used interchangeably here forth and will carry the same meaning. Frame detection is used to determine the symbol boundary so that correct samples for a symbol frame can be taken. Any deviation from this boundary (timing instant) means that the sensitivity to delay spread increases, so the system can handle less delay spread than what it was initially designed to accommodate. With this, any OFDM system should be design such that the timing error is small compared to the guard interval in order to maintain robustness.

The FFT time synchronization error can be modelled as a shift in the interval of integration of the matched filter. For a timing error of δt the interval $t \in [kT, kT + T_{FFT}]$ becomes $t \in [kT + \delta t, kT + T_{FFT} + \delta t]$ [11].

$$y_{i,k} = \frac{1}{T_{FFT}} \int_{t=kT+\delta t}^{kT+T_{FFT}+\delta t} r(t) e^{-j2\pi(t-kT-\delta t)/T_{FFT}} dt$$

(2-6)

The OFDM transceiver should be designed such that $\delta t < T_{guard}$, in which no ISI occurs as a result of FFT time synchronization error. From (2-3), the following is obtained.

$$y_{i,k} = \sum_{i'=-N/2}^{N/2-1} x_{i,k} \frac{1}{T_{FFT}} \int_{u=0}^{T_{FFT}} \left[\int_{\tau=0}^{\tau_{max}} h_k(\tau) e^{-j2\pi i'\tau/T_{FFT}} d\tau \right] e^{-j2\pi[(t-t')u+t'\delta t]/T_{FFT}} du$$

$$+ n_{i,k}$$

(2-7)

With his, the expression for the demodulated signal constellations in case of a timing error is given by

$$y_{i,k} = x_{i'k} h_{i'k} e^{-j2\pi i \delta t / T_{FFT}} + n_{i,k} = x_{i'k} h_{i'k} e^{-j2\pi i \delta t' / N} + n_{i,k}$$

(2-8)

It is clear that a timing offset will cause a progressive phase rotation from examining (2-8). The phase rotation is zero at the centre frequency and it increases linearly towards the edges of the frequency band. It can be verified that a timing-offset of one sample introduces a phase shift of $\pm \pi$ to the outermost sub-carriers (having i $\cong \pm N/2$), regardless of the FFT-length [11].

2.6.2 Carrier Synchronization Error

Carrier synchronization errors occur because of a small deviation of frequency between the local oscillator in the transmitter and receiver. It can also be due to Doppler effect when mobility is considered. This can be visualized as an error in

frequency instant, where the signal is sampled during demodulation via FFT. The carrier offset can be modelled as a frequency shift δf and phase shift θ in the received signal. Incorporating all these into (2-3), the following is obtained.

$$
y_{i,k} = \frac{1}{T_{FFT}} \int_{i=kT}^{kT+T_{FFT}} r(t) e^{j(2\pi\delta f t+\theta)} e^{-j2\pi(t-kT-\delta t)/T_{FFT}} dt
$$

$$
= e^{j2\pi\theta} \frac{1}{T_{FFT}} \int_{i=kT}^{kT+T_{FFT}} \left[\int_{\tau=0}^{\tau_{max}} h(\tau)s(t-\tau)d\tau + n(t) \right] e^{j2\pi\delta f t} e^{-j2\pi(t-kT-\delta t)/T_{FFT}} dt
$$

$$
= e^{j(\theta+2\pi\delta f kT)} \sum_{i'=-N/2}^{N/2-1} x_{i',k} h_{i',k} \frac{1}{T_{FFT}} \int_{u=0}^{T_{FFT}} e^{-j2\pi\left(\frac{i-i'}{T_{FFT}}-\delta f\right)u} du + n_{i,k}
$$

(2-9)

From (2-9), it can be seen that the desired amplitude of the constellation points will be decreased and there will be contributions from adjacent subcarriers, leading to ICI. The integration will not be 1 for $i = i'$ and neither is it 0 for $i \neq i'$, hence there will be a lost of orthogonality between subcarriers.

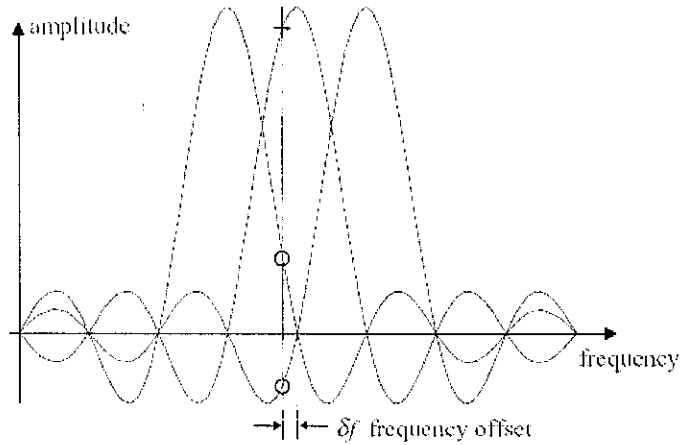Figure 11   Inter-carrier-interference (ICI) arises in case of a carrier synchronization error.

The ICI term can be seen as an additional noise term and can thus be represented as a degradation of SNR [11]. Evaluation of the phase rotation and attenuation due to a frequency error yields

$$
y_{i,k} = x_{i,k} h_{i,k} \sin c(\delta f T_{FFT}) e^{\{j[\theta+2\pi\delta f(kT+T_{FFT}/2)]\}} + n'_{i,k}
$$

(2-10)

23

Since

$$\frac{1}{T_{FFT}} \int_{t=0}^{T_{FFT}} e^{j2\pi\delta f t} dt = \frac{1}{j2\pi\delta f T_{FFT}} \left[e^{j2\pi\delta f T_{FFT}} - 1 \right]$$

$$= e^{j2\pi\delta f T_{FFT}} \frac{\sin \pi \delta f T_{FFT}}{\pi \delta f T_{FFT}}$$

$$= e^{j2\pi\delta f T_{FFT}} \sin c \pi \delta f T_{FFT} \qquad (2\text{-}11)$$

2.6.3 Common Carrier and Timing Offset

Synchronization errors involve both FFT time synchronization error and carrier synchronization error. The synchronization errors in the system transfer function can be generalized as follows.

$$y_{i+\delta f_i,k} = x_{i,k} h_{i,k} \sin c \left[(\delta f - \delta f_i F) T_{FFT} \right] e^{j\psi_{i,k}} + n'_{i,k} \qquad (2\text{-}12)$$

where

$$\psi_{i,k} = \theta + 2\pi\delta f \left(kT + \frac{T_{FFT}}{2} + \delta t \right) + 2\pi\delta t \frac{i}{T_{FFT}} \qquad (2\text{-}13)$$

Expressing (2-13) in terms time samples

$$\psi_{i,k} = \theta + 2\pi\delta f' \left(\frac{1}{2} + k \frac{N + N_{guard} + N_{win}}{N} + \frac{\delta t'}{N} \right) + 2\pi\delta t' \qquad (2\text{-}14)$$

24

CHAPTER 3

METHODOLOGY

OFDM signal in time domain looks like a Gaussian noise because it is the superposition of many subcarriers with random phases and amplitudes depending on user data. The subcarriers are spaced closer and closer together in frequency domain when the number of subcarriers is increased to provide better data rate considering that the available bandwidth is the same [12]. This brings the need for stricter synchronization in the system. Thus, synchronization is one of the most critical topics since OFDM demodulation is virtually impossible with minute synchronization error. This notion is supported by most references listed.

For high-rate packet transmission, the synchronization time needs to be as short as possible, preferably an OFDM symbols only. To achieve this, special OFDM training symbols can be used to achieve better synchronization. Each WiMAX IEEE 802.16 frame is preceded by a preamble (training symbol) [3], a sequence of samples whose purpose is to allow detection, synchronization and training The length and the contents of the preamble have been carefully designed to provide enough information for good synchronization performance [16]. A discussion about the design of the training symbol is presented in the next section. With that, an explanation about the functions of the receiver and its constituent components are given before an analysis of current synchronization algorithms. This chapter is concluded with the proposal of a new hybrid synchronization algorithm that is more robust.

3.1 Design of the Training Symbol

The design of the training-symbol is base on the work of Schmidl and Cox [10] on frequency and time synchronization for OFDM. The first of the two training symbols (TS) used in [10] is a unique OFDM symbol because every alternate subcarrier (SC)

is zero. This implies that the symbol has identical halves in the time-domain, due to properties of the Fourier transform (*cf* Appendix B).

In the original scheme [10], the odd-numbered subcarriers are zero, while the even subcarriers contain a known, binary pseudo noise (PN)-sequence. Analyzing Table 1 of Section 2.5, it is seen that many of the even-numbered sub-carriers must be zero, because they are used to separate sub-bands and to avoid problems with DC-offsets and carrier feed-through [11]. In order to apply the synchronization scheme to this OFDM system, odd-numbered sub-carriers are use to contain the PN-sequence. This is a novel modification of the well-known technique. Nevertheless, the corresponding time-domain symbol has identical halves, but the samples of its second half have opposite signs, which are easily taken into consideration in the estimation steps [11].

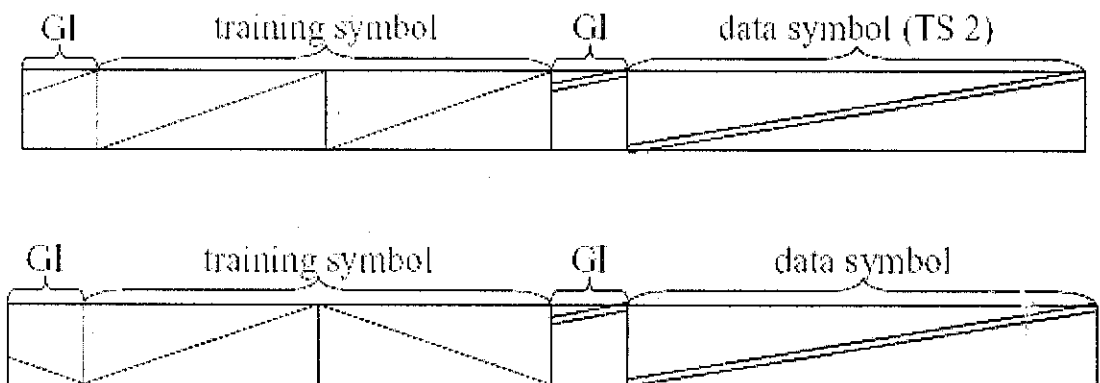Figure 12   Structure of the training symbol. Top: Original Schmidl and Cox scheme. Bottom: Proposed method

In [10], two OFDM symbols comprise the training sequence. Known data is modulated there differentially between the two OFDM symbols, for the purpose of integer frequency- synchronization. With this, the modification used here therefore reduces the overhead introduced by one OFDM symbol per frame [17].
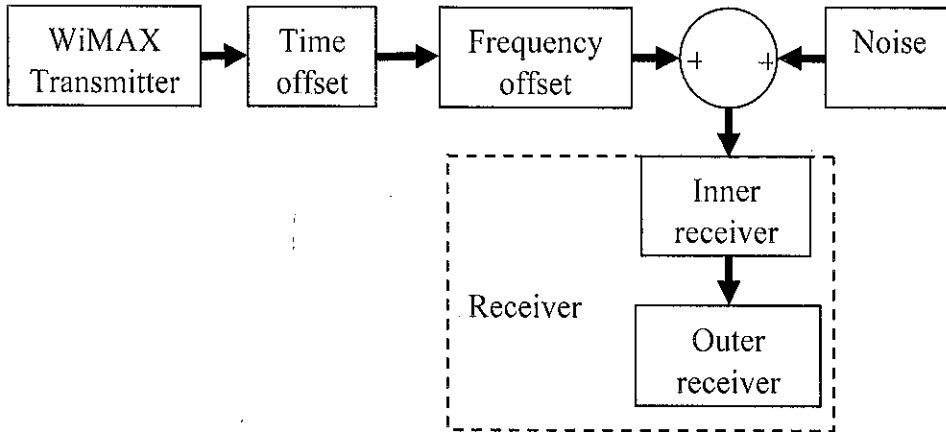
3.2 Simulation Work

Figure 13   Implementation (blockset only) in Simulink

The WiMAX transmitter and receiver will be implemented in MATLAB/Simulink. OFDM frames which are preceded by the training symbol are continuously broadcasted by the transmitter. The WiMAX/OFDM signal will then be subjected to a time and frequency offset before being superimposed with AWGN (additive white Gaussian noise). A time offset can be modelled as a deliberate delay introduced before the receiver. On the other hand, frequency offset can easily be inserted using the phase/frequency offset block readily available in Simulink. A frequency offset can be visualized as a rotation of the constellation points. With this, the signal with deliberately added distortions is passed on to the receiver. The deliberate offsets and distortions are necessary to ensure the receiver is totally "blind". Only with this prerequisite, the synchronization algorithms can be verified.

The receiver is divided to an inner and outer part (Figure 13 and 14). The inner receiver involves pre-FFT processing. First, the frame timing synchronization blockset will try to identify the start of the OFDM frame (cf Section 3.3). Subsequently, the frequency synchronization (cf Section 3.4) blockset will determine the frequency offset and then multiply the received signal with a correction factor. These two synchronization steps need to be a pre-FFT process for it to be rapid. If these synchronization steps were to be performed post-FFT, the transform itself would introduce considerable delay. The RF front end is shown for completeness sake.
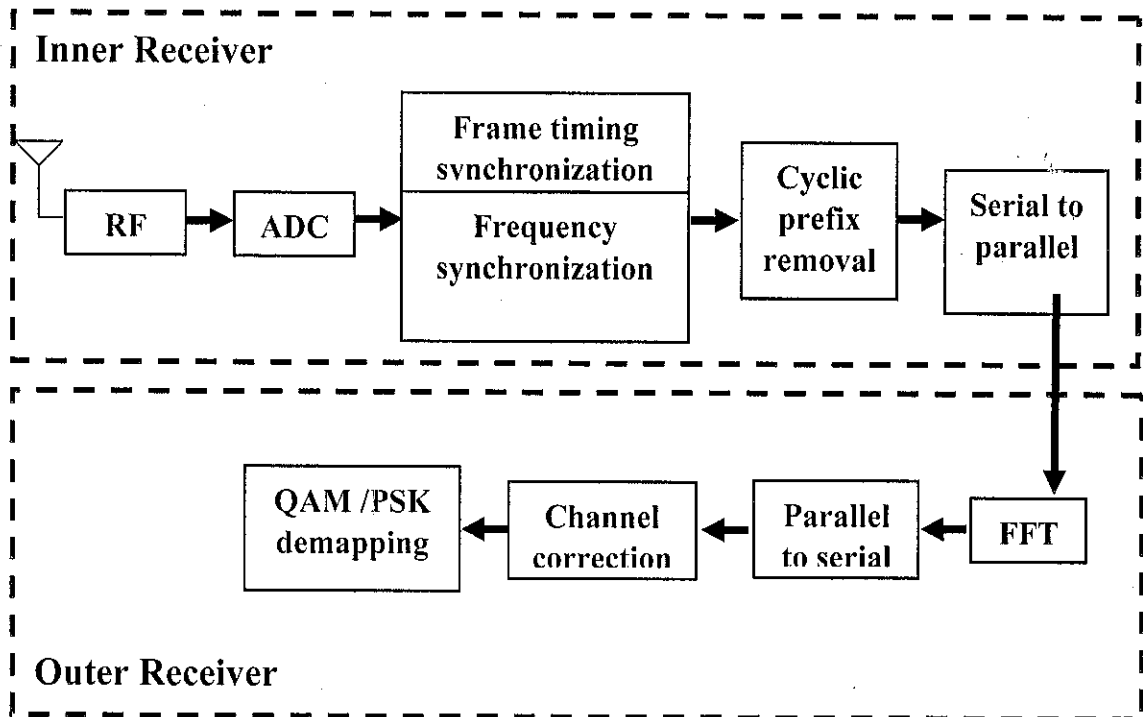
27

Figure 14   WiMAX/OFDM receiver structure

The compensated signal is then used to decode the transmitted data in the outer receiver. The outer receiver involves post-FFT processing. Actual demodulation is achieved via FFT (Figure 14), which is performed on all the orthogonal subcarriers. The channel correction operates on demodulated OFDM symbols. This blockset will estimate the channel coefficient and then multiply the demodulated symbols with its inverse. No implementation of this blockset is carried out in this work but is only mentioned in passing in this report. The output of the FFT is QAM/PSK constellation points which are mapped onto binary values. After that, these values are decoded to recover the transmitted data.

In order to successfully interpret the QAM/PSK constellation points, the reference phase and amplitude of all subcarriers need to be ascertained first. Alternatively, differential techniques can be applied [8].

3.3 Frame Timing Synchronization

Two methods can be adopted to achieve frame timing synchronization in the inner receiver. The first is Schmidl and Cox technique [10]. In fact, this method is the de-facto method in most conventional OFDM receivers. The second method is double sliding window packet detection. This method is not an OFDM mainstream technique but is proven to be effective in getting the job done (*cf* Chapter 4).

3.3.1 *Schmidl and Cox Technique*

The Schmidl and Cox [10] technique incorporates a sliding window correlator in addition to an energy detector used to normalize the decision statistic and hence guard against fluctuations of the received signal power [22]. A sliding window P computes the cross-correlation between the received signal and a version of the delayed (by one short preamble) received signal. Another sliding window R is used to compute the received signal energy within the cross-correlation interval.

Let there be L-1 $(L = \frac{N}{2})$ complex samples in one-half of the first training symbol (excluding the cyclic prefix), and let the sum of the pairs of products be

$$P(d) = \sum_{i=0}^{L-1} \left(r_{d+i}^{*} r_{d+i+L} \right)$$

(3-1)

which can be implemented with the iterative formula

$$P(d) = P(d-1) + r_{d+L-1}^{*} r_{d+2L-1} - r_{d-1}^{*} r_{d+L-1}$$

(3-2)

Note that d is a time index corresponding to the first sample in a window of $2L$ samples. This window slides along in time as the receiver searches for the first training symbol. The received energy for the second half-symbol is defined by

$$R(d) = \sum_{i=0}^{L-1} \left| r_{d+i+L} \right|^2$$

(3-3)

which also can be implemented iteratively as

$$R(d) = R(d-1) + \left| r_{d+2L-1} \right|^2 - \left| r_{d+L-1} \right|^2$$

(3-4)

With this, the decision statistic, $M(d)$, is given by:

$$M(d) = \frac{\left| P(d) \right|^2}{(R(d))^2}$$

(3-5)

The decision statistic reaches a plateau which has a length equal to the length of the guard interval minus the length of the channel impulse response. The start of the frame can be taken to be anywhere within this window without a loss in the received SNR [10] but the optimum timing, d_{opt}, is obtained at the end of the plateau.
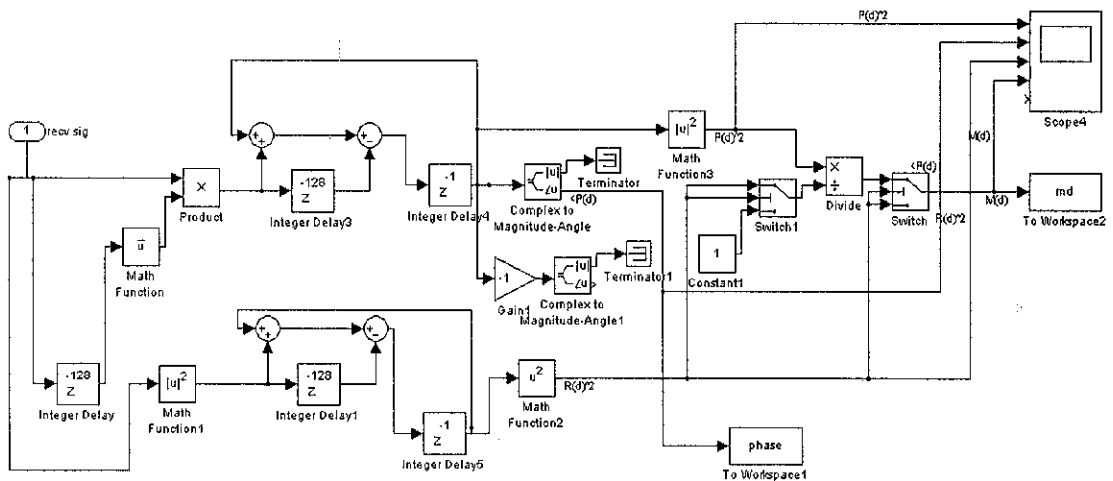

Figure 15   Implementation of Schmidl and Cox technique in Simulink

Figure 15 show how the above equations are realized in Simulink. $P(d)$ and $R(d)$ are implemented in a hardware efficient manner according to (3-2) and (3-4). With this, the computations require just one complex multiplication and two additions/ subtractions per input sample respectively. In addition, there is a control circuit to ensure that the problem of divide by 0 does not occur.

3.3.2 Double Sliding Window Packet Detection

The underlying principle of the double sliding window packet detection algorithm is to form the decision variable m_n as a ration of the total energy contained inside the two windows. Therefore, the receiver does not need to know the absolute value of the received energy [11].
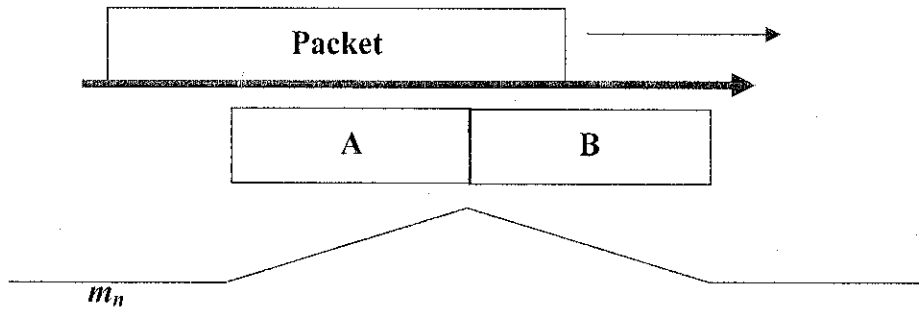
Figure 16   Illustration of the double sliding window packet detection

Let the energy inside A and B be

$$a_n = \sum_{m=0}^{M-1} r_{n-m} r^*_{n-m} = \sum_{m=0}^{M-1} \left| r_{n-m} \right|^2$$

(3-6)

$$b_n = \sum_{l=0}^{L-1} r_{n-l} r^*_{n-l} = \sum_{l=0}^{L-1} \left| r_{n-l} \right|^2$$

(3-7)

M and L are the window sizes of a_n and b_n respectively and are usually made the same. With this, the decision variable is given by

$$m_n = \frac{a_n}{b_n}$$

(3-8)

The peak $E[m_n]$ occurs when index n is exactly the start of the packet (i.e. a_n would consist of signal and noise and b_n would consist purely of noise) [15].

$$E[m_n]_{peak} = SNR + 1$$

(3-9)

31

Thus, locating the peak of m_n would provide the expected start point of the packet. The following figure shows the implementation in Simulink. It also incorporates the circuitry to prevent divide by 0 problems.
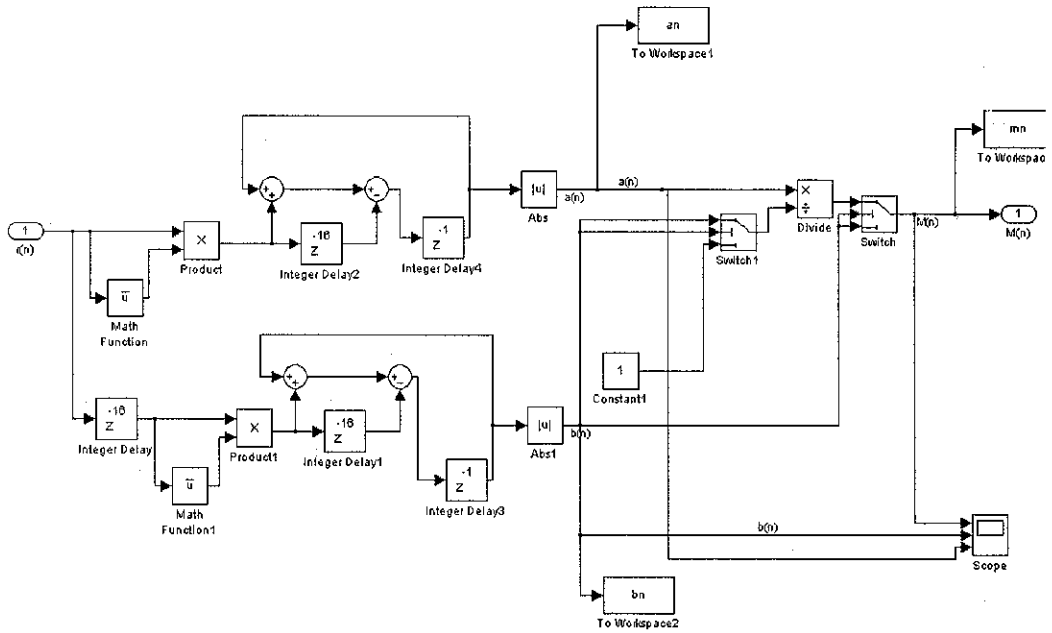

Figure 17   Implementation of double sliding window packet detection algorithm in Simulink

3.4   Frequency synchronization

The algorithm for frequency-synchronization is based on the fact that the phase-angle of the above-defined correlation sum at its optimum position, $P(d_{opt})$, is proportional to the carrier frequency-offset, as seen from the following derivation. The received signal with frequency offset can be modelled as

$$r_i = s_i e^{j(2\pi\delta f' i + \theta)}$$

(3-10)

where $\delta f'$ is the frequency-offset normalized to the subcarrier spacing F, and θ is the carrier phase offset. For small frequency offsets, $\delta f'$ less than π, then the frequency offset estimate is

32

$$\hat{\delta f} = \frac{1}{\pi} \angle [-P(d_{opt})]$$

(3-11)

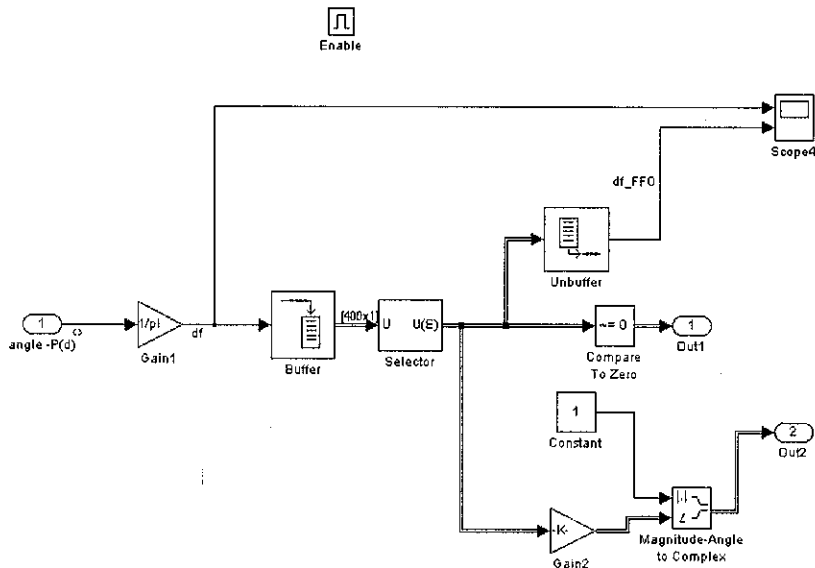For the proof of (3-11) *cf* Appendix B).

Figure 18   Implementation of frequency synchronization algorithm in Simulink

Figure 18 shows the implementation in Simulink. After obtaining the frequency offset estimates, synchronization is achieved my multiplying the samples by $e^{-j2\hat{\delta f}'/T}$.

3.5   Proposed Synchronization Algorithm

Analysis of the Schmidl and Cox technique will reveal its not so satisfactory performance for frame timing synchronization when channel SNR is low (*cf* Section 4.2.1). In fact, it is quite a well known fact that there will always be an uncertainty in determining the optimum timing via this technique. Nevertheless, this method performs very efficiently for frequency synchronization. On the other hand, the double sliding window has been proven to be accurate in identifying the start of a frame (*cf* Section 4.2.3).
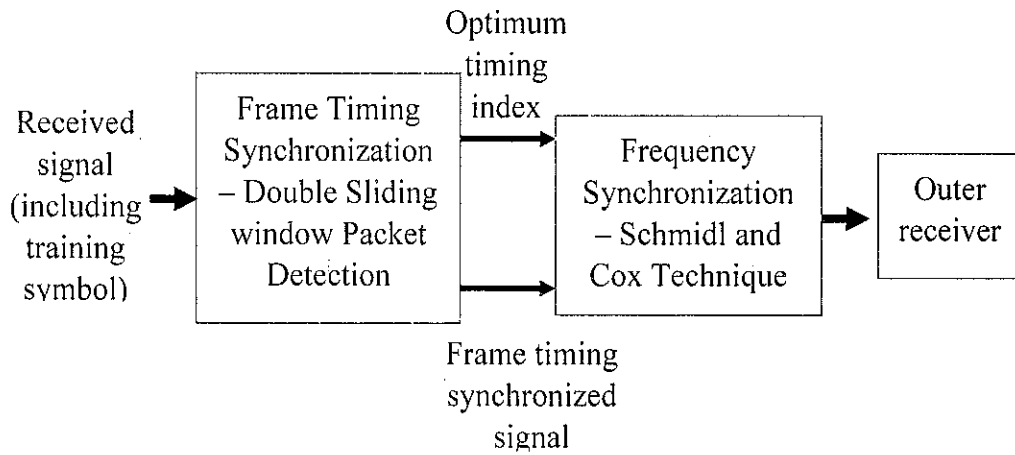
33

Figure 19 Overview of the proposed algorithm

With this, the proposed algorithm attempts to make the Schmidl and Cox technique more robust. This is possible by adopting the double sliding window packet detection for frame timing synchronization. The Schmidl and Cox technique is left to handle the frequency synchronization portion. Hence, there is no need to compute the $R(d)$ component and there is no need to incorporate any heuristics to determine optimum timing. Consequently, the optimum timing index will be obtained from the double sliding window packet detection blockset. Therefore, the angle $P(d)$ that corresponds to the optimum timing index is indeed a fix position.

CHAPTER 4

RESULTS AND DISCUSSION

Having elaborated on the synchronization algorithms and its implementations, this chapter presents the results from the simulation work. This encompasses time domain plots of the WiMAX / OFDM signal and corresponding decision metric plots. For all time domain plots, the *y-axis* represents amplitude and *x-axis* represents sample index. In addition, some frequency domain/phasor plots i.e. constellation point diagrams are also presented. All simulation results are obtained with the following parameters. Symbol length of 320 points i.e. cyclic prefix occupying 64 preceding points and DBPSK modulation format. The AWGN channel of non-dispersive nature of is used in all simulations with SNR that are specified per case. In a nutshell, the proposed algorithm managed to work as intended. It can achieve accurate synchronization even in low SNR.

4.1 The training symbol

By modulating a PN-sequence on every consecutive subcarrier, odd in this case, a training symbol with equal halves and opposite signs was generated. Figure 20 and Figure 21 illustrate the training symbol in the time domain.
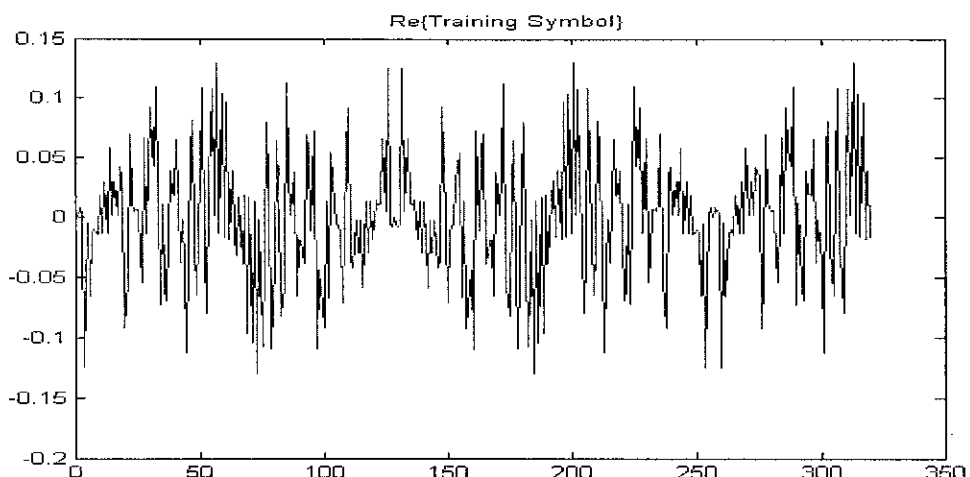

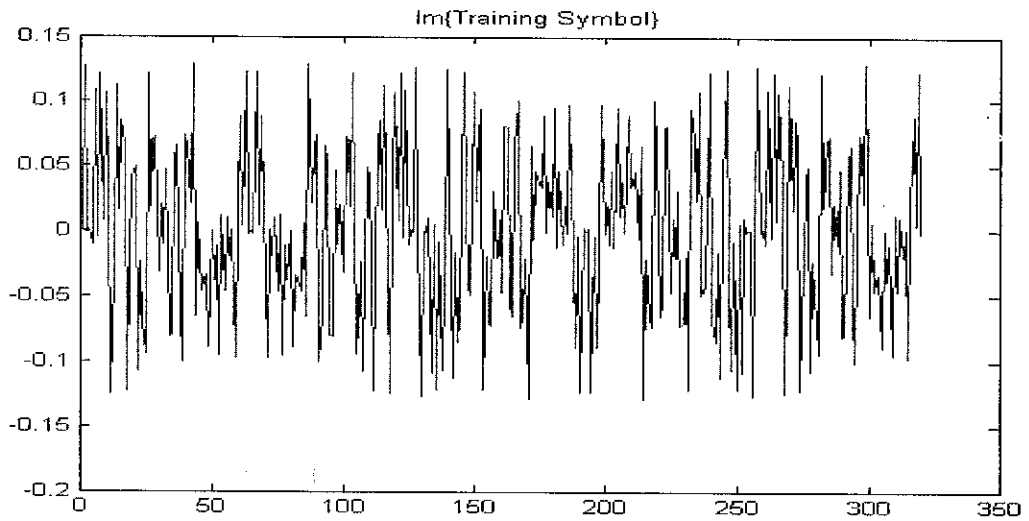Figure 20   Real part of the training symbol

35

Figure 21   Imaginary part of the training symbol

In order to demonstrate the property of equal halves in time domain but with opposite signs, note that $x[n+N/2] = -x[n]$. With this, $x[n] + x[n+N/2] = 0$, and this is confirmed with the following plot.
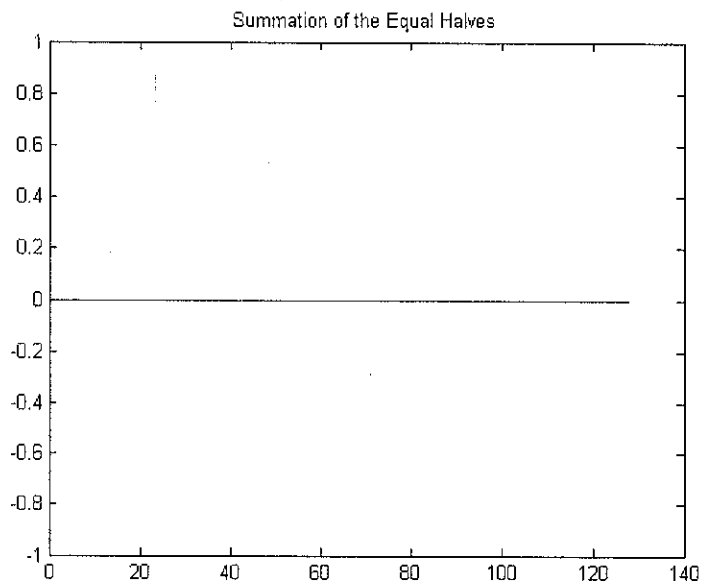

Figure 22   Summation of the equal halves in time domain

4.2 Frame Timing Synchronization

In this section, both results for both Schmidl and Cox technique and double sliding window packet detection are presented.

4.2.1 Schmidl and Cox Technique

In a perfect channel (noiseless), for values of d before the start of the frame, $M(d) = 0$ (Figure 23). When d is within start of the frame until $N/2$, $M(d)$ starts to increase. For the next few samples spanning the length of the cyclic prefix, $M(d)$ takes the value of 1. As d increase beyond this point, $M(d)$ decreases to 0. The flat top of or plateau of $M(d)$ is due to the guard interval, because the cyclic prefix also has equal samples at the required correlation-lag (in a non-dispersive channel). The optimum timing is obtained at the end of the plateau. Although the start of the frame can be taken to be anywhere within the plateau without a loss in the received SNR [10], this can easily lead to misdetection and also false detection especially in low SNR.

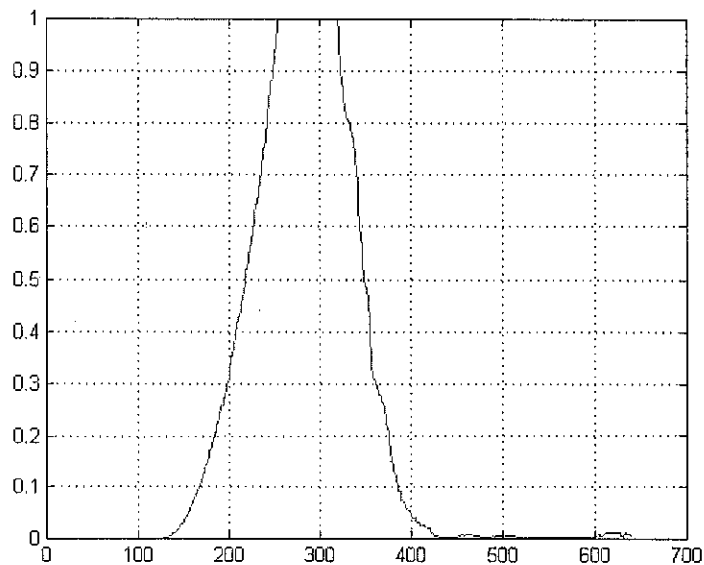Figure 23   Example of the timing metric for a perfect channel

Detecting the optimum timing i.e. end of the plateau is quite a trivial task in ideal conditions or high SNR channel (Figure 24). Nevertheless, the existence of a plateau is not so prominent in the case when channel SNR is low. This point is illustrated in Figure 25. The plot shows the $M(d)$ metric obtained via the Schmidl and

37

Cox method in a non dispersive AWGN channel with an SNR of 9.4 dB as recommended by [3].
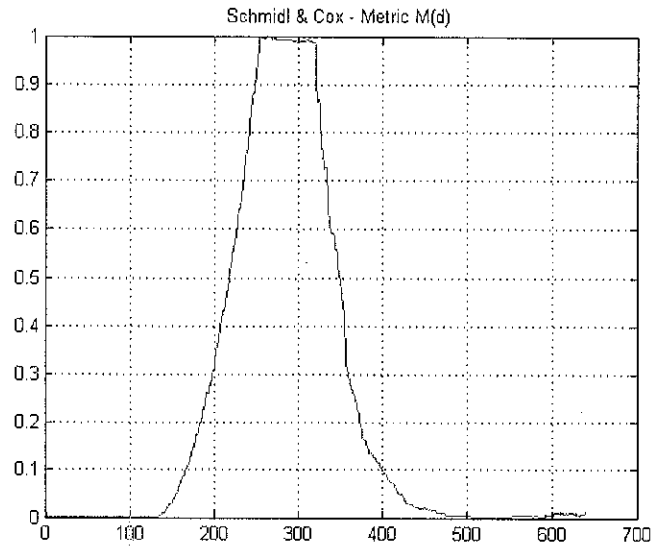

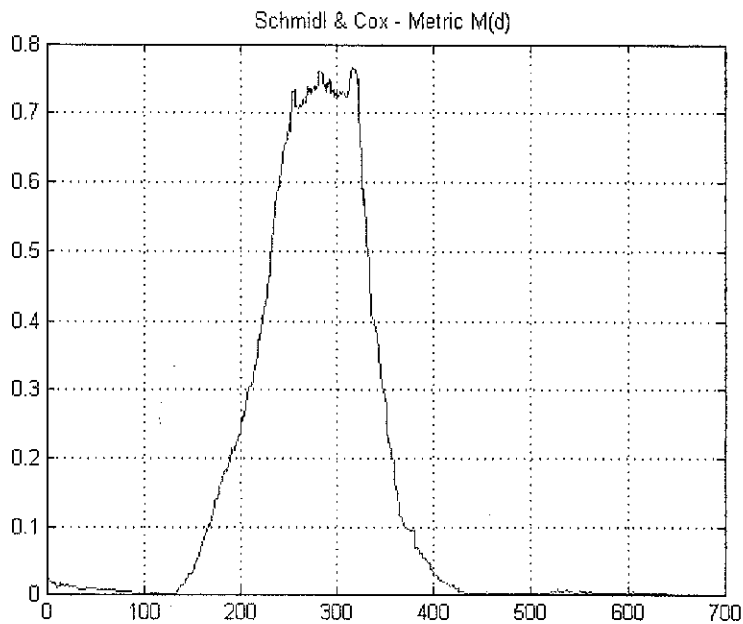Figure 24   *M(d)* metric, SNR = 30 dB

Figure 25   *M(d)* metric, SNR = 9.4 dB

When this is the case, determining the optimum timing proves to be a difficult task. A lot of heuristic needs to be developed in order to intelligently ascertain the start of an OFDM frame. Numerous methods were proposed by different authors. For example,

1. Filtering for the longest peak during the frame [9]. This is because the plateau at the optimum position always has considerable length.

2. Comparing $M(d)$ against a threshold value. If greater or equal to this threshold value, a preamble symbol is deemed to have been received. The symbol start is calculated as being ¼ of the way between the counter (exceeding threshold) start and stop samples [23].

With this, it is clear that the Schmidl and Cox technique does not perform well under low SNR scenarios. The difficulty in identifying the optimum timing (at the end of the plateau) can jeopardize the accuracy of other synchronization process. Thus, this method is not so suitable for frame timing synchronization. As an alternative, double sliding window (next section) is proposed to handle this synchronization step.

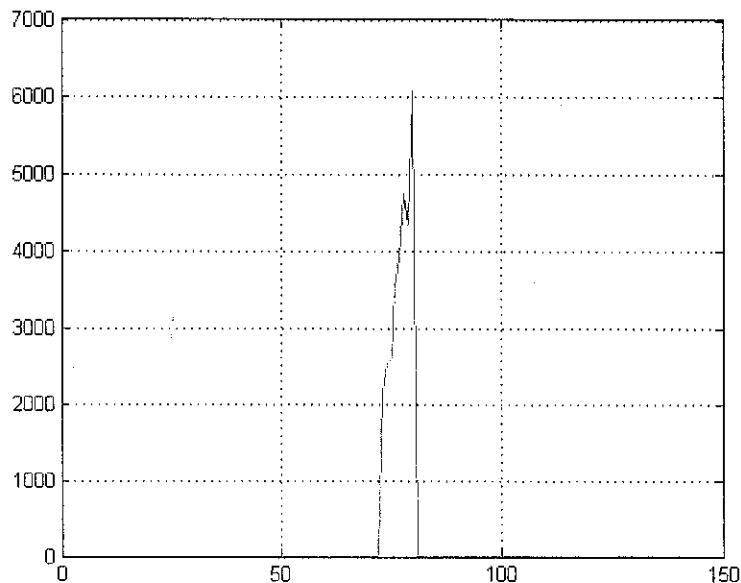### 4.2.2 Double Sliding Window Packet Detection

Figure 26 m_n metric, SNR = 30 dB

Figure 26 shows the decision metric for the double sliding window packet detection for a non dispersive AWGN channel of 30 dB SNR i.e. high SNR. From (3-6), (3-7) and (3-8), m_n will balloon up to an infinite value when the channel is noiseless.

Hence, there is no such a plot for noiseless channel. For a lag of l which is less than the start of frame, the metric is around the value of 1. When the OFDM frame starts to slide into window A, the metric starts to rise. A peak is reached when the whole of window A is filled with the OFDM frame. After that, the metric starts to decline as the frame also start to fill up window B. By observation, it is very easy to identify the start of the OFDM frame. The lag that maximizes the metric or in other words the index of the peak of the metric is chosen as the optimum timing. Even in low SNR i.e 9.4 dB (Figure 27), there is no ambiguity in ascertaining the start of a frame. Double sliding window packet detection method always produces a sharp peak even in cases where SNR is below 9.4 dB. However, these conditions do not permit proper and normal data transmission. Hence, conditions of too low SNR is not considered.
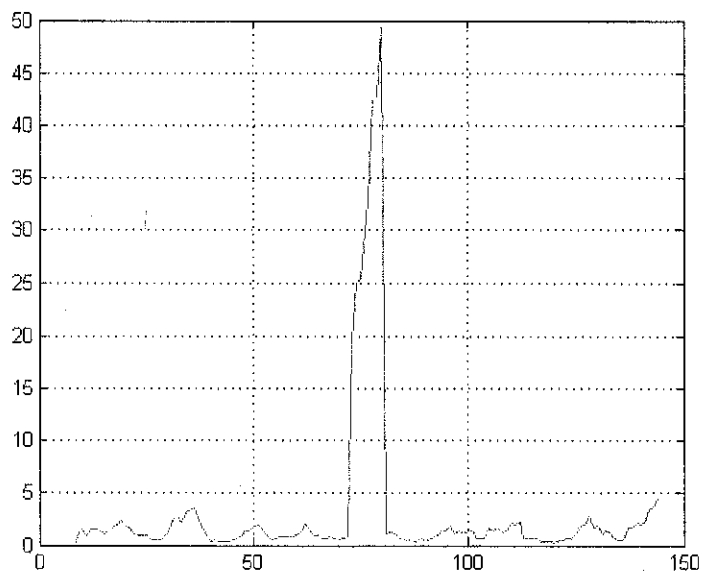
Figure 27 m_n metric, SNR = 9.4 dB

4.2.3   Comparison between both algorithms

Figure 28 shows the metric for both Schmidl and Cox and double sliding window methods. The channel is a non dispersive AWGN with an SNR of 9.4 dB as recommended by [3]. The Schmidl and Cox metric does not even show any clear existence of a plateau. This scenario can lead to misdetection. On the other hand, the double sliding window metric still shows a sharp peak. The double sliding window metric is normalized to the peak value in order to show comparison against the

Schnidl and Cox metric. Base on this observation, the double sliding window is the superior method of frame timing synchronization. What remains after locating the peak would be to align the received signal to the index that corresponds to this peak. Provided that a peak exists in the double sliding window metric, the start of frame identified is very accurate. Hence, the cyclic prefix can also be stripped away in an accurate fashion.
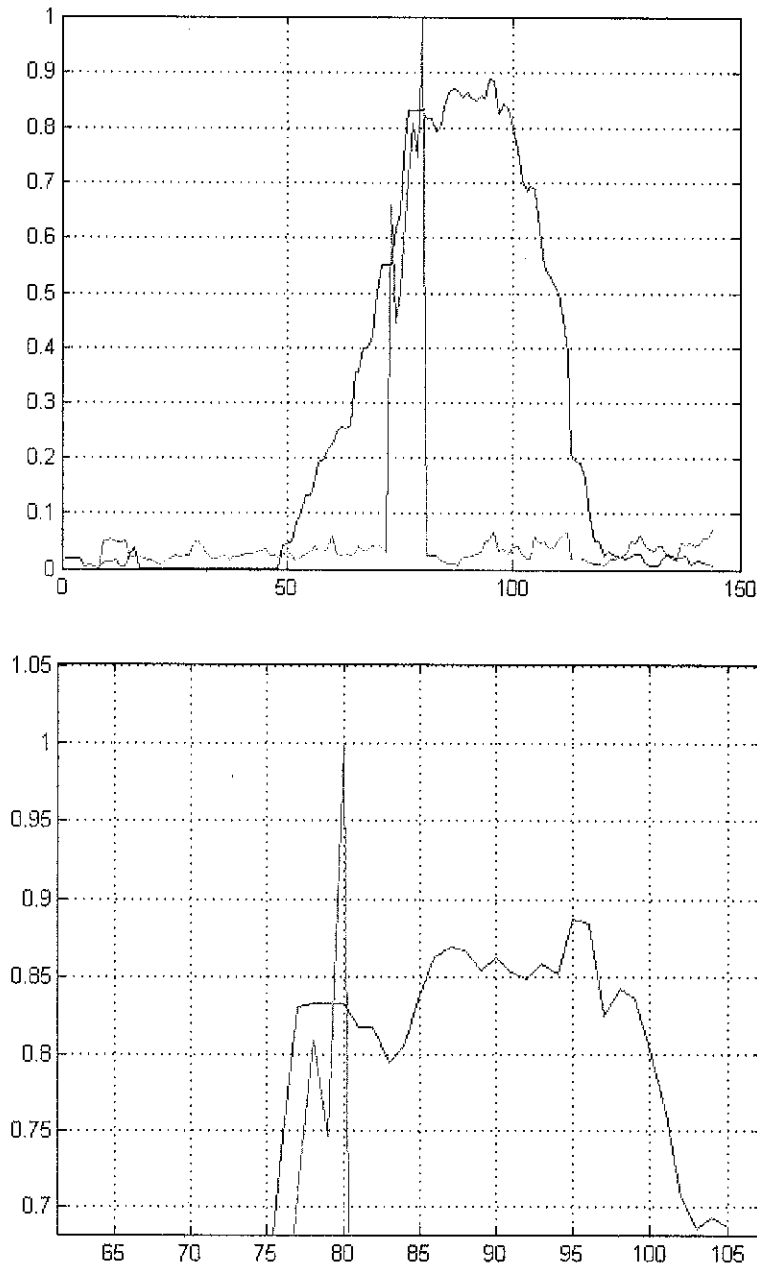

Figure 28   Decision metric for both methods, SNR = 9.4 dB. The double sliding window method produces a sharp peak. Exact frame start is at the 80 index. Bottom: A close up view

41

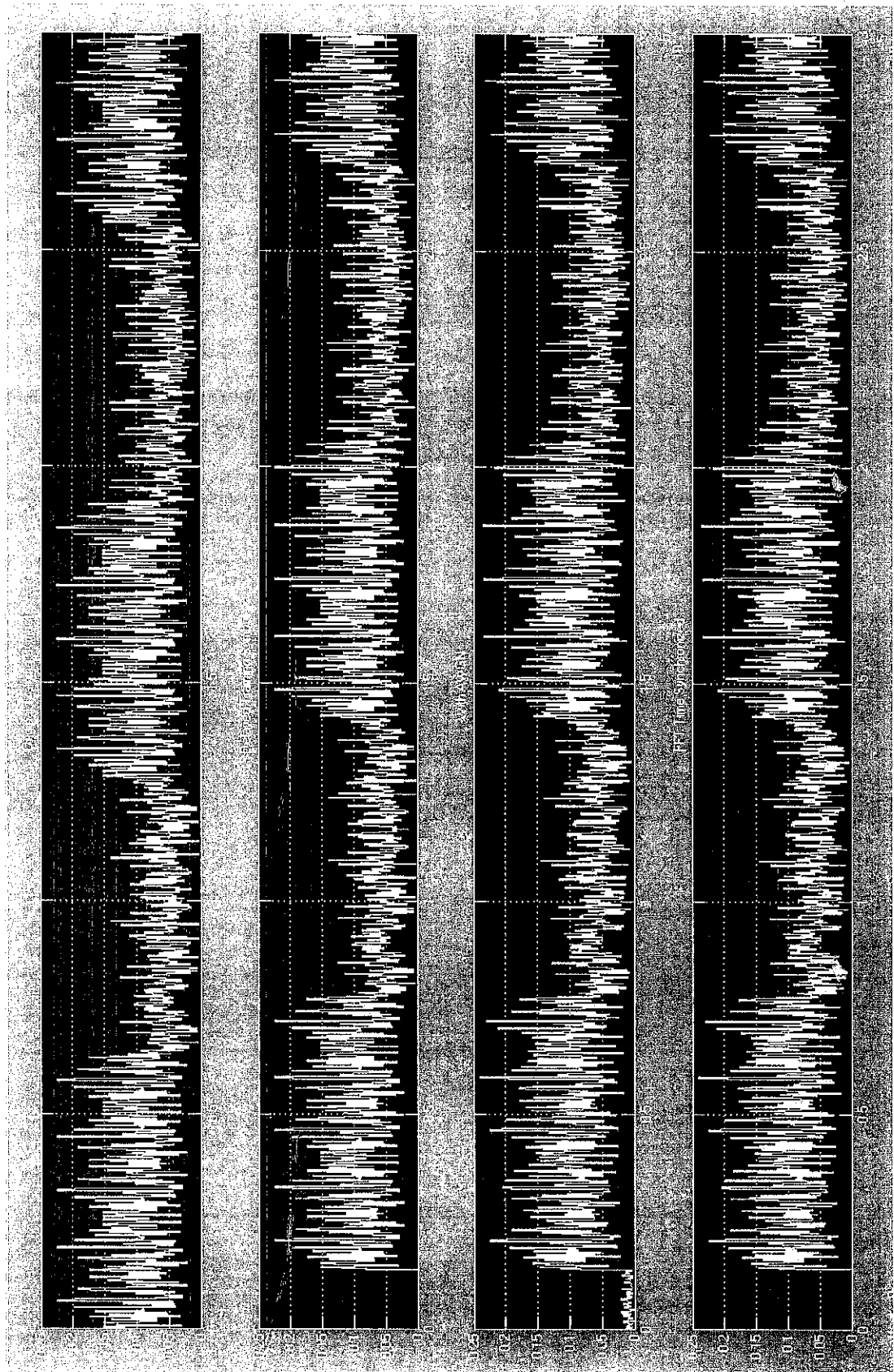## 4.3 Results for Proposed Method

Figure 29   Various time domain plot for the proposed algorithm

Figure 29 shows the various time domain plots (magnitude only) for the proposed algorithm. The first plot illustrates the original version (undistorted) of the training symbol and random OFDM data. This frame consists of one preamble (training symbol) and one data symbol. Note that the signal looks like Gaussian noise. The preamble part is the slightly larger in amplitude and starts from time 0. Coincidently, the preamble is also slightly amplified in the IEEE 802.16 [3]. The next vertical plot shows the signal with deliberate delay added. From observation, the signal no longer starts at the beginning of the simulation. This will create the effect of a "blind" receiver since it has no a priori knowledge of when the signal actually begins.

The third vertical plot depicts how the signal would look like when it passes through the AWGN channel. From observation, the signal is distorted and does not resemble the original version 100 percent. The final vertical plot shows the signal after frame timing synchronization. Note that the AWGN noise preceding the preamble is no longer there. The algorithm has managed to successfully identify the start of the frame.

4.4 Frequency Synchronization

The Schmidl and Cox method is used to take care of the remaining synchronization tasks. From the plot of angle of $P(d)$ (Figure 30 top), it can be observed that the value is constant over where the "plateau" (although not that prominent) exists for the $M(d)$ metric. Hence, actually any point there can be chosen as the fractional frequency offset. Nevertheless, the optimum point would correspond to the angle of $P(d)$ at the optimum timing i.e. at the end of the $M(d)$ plateau. The value obtained here is actually proportional to the subcarrier spacing. For a bandwidth of 20 MHz, this algorithm can correct a drift of up to a maximum of 39 062.5 Hz (cf Section 3.4).
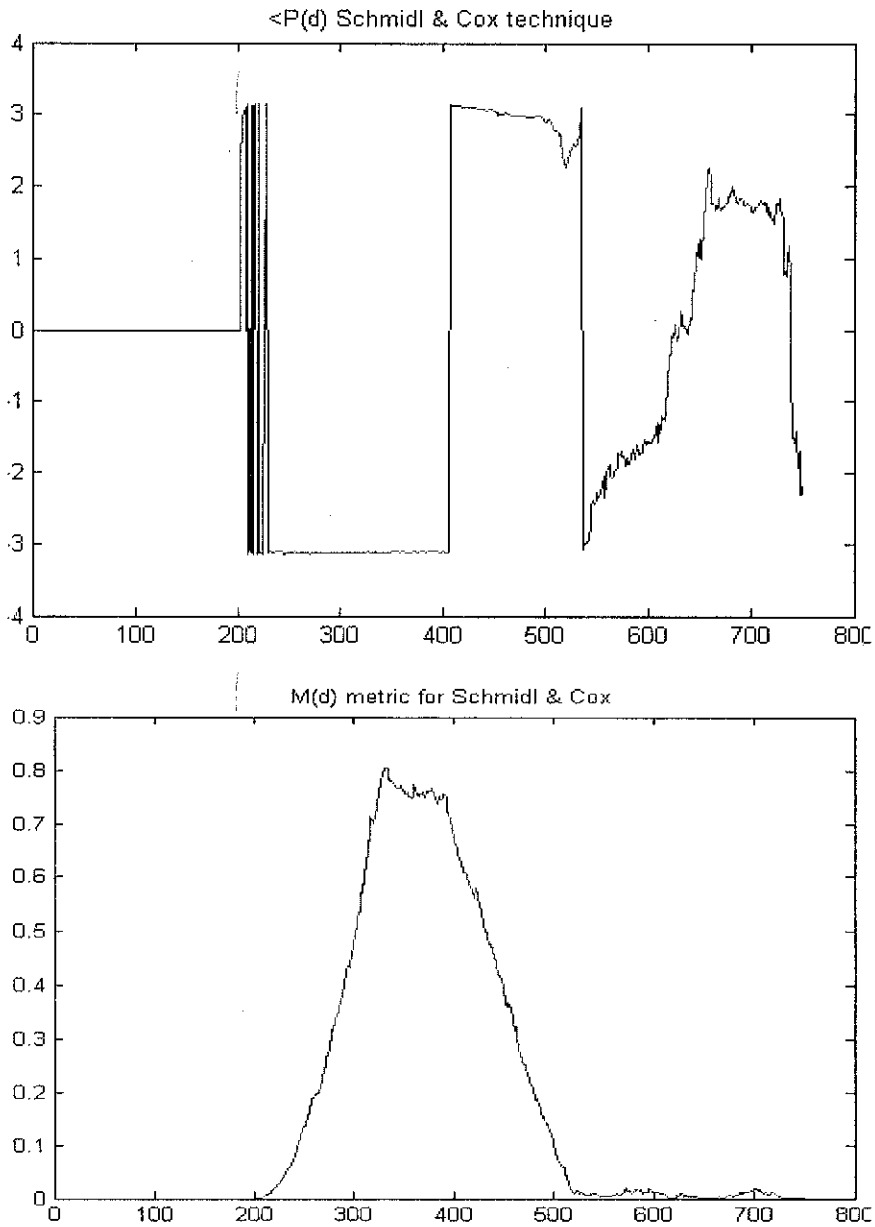
Figure 30   Angle of *P(d)*. Bottom: M(d) is shown for orientation purposes

Figure 31 illustrates the effect of a frequency offset of 1/16 subcarrier spacing on the constellation points. Basically, the constellation points will start spinning around the origin. When this occurs, demodulation would result in chaos since orthogonality is lost between subcarriers. Figure 32 shows the constellation points after frequency synchronization. With this, the points no longer spin but are located about the +/-1 due to AWGN noise.

Figure 31   Constellation diagram for frequency offset = 1/16 subcarrier spacing without synchronization

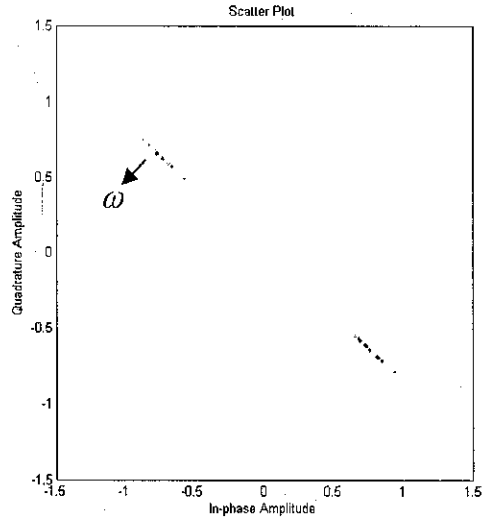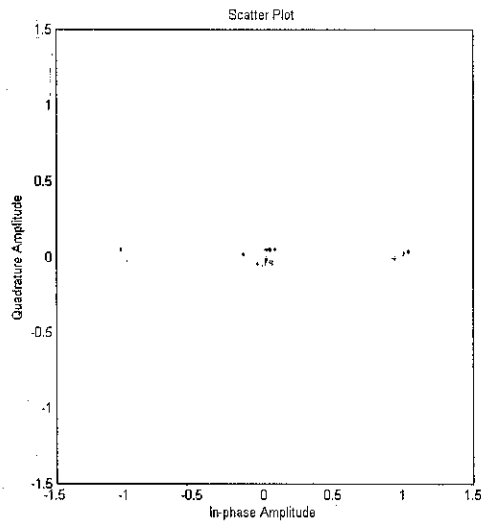Figure 32   Constellation diagram for frequency offset = 1/16 subcarrier spacing with synchronization

CHAPTER 5

CONCLUSION AND RECOMMENDATION

5.1   Recommendations for Synchronization Algorithm

In order to further improve the accuracy and reliability of the current proposed algorithm, the metric for double sliding window can be coupled with some threshold of $P(d)$. This would mean that only when $P(d)$ rises above a certain threshold and when a peak is detected via the double sliding window, then it is assumed that it is the correct start of a frame. With this, the probability of false detection is minimized.

Another suggestion would be to normalize the $M(d)$ metric of the double sliding window. This is because from the results, it can see that this metric increases to a magnitude of more than 1000 and beyond when channel SNR is high. Hence, clipping will occur especially in fixed-point implementation environment. Accuracy is then compromised. With this, it is clear that a normalization mechanism for this metric is necessary.

5.2   Recommendations for Future Work

The simulation work can be mode more complete by incorporating a SUI (Stanford University Interim) channel. This will render the model to be more realistic since the SUI channel is a time dispersive channel and is specified in IEEE 802.16 [3]. Subsequently, a channel estimation and correction algorithm is needed to mitigate the effects of the time dispersive nature of the channel.

This project can be brought to the next level via hardware implementation. In fact, there is only one step left before hardware realization i.e. conversion from Simulink blocksets to Xilinx blocksets. With the assistance of ModelSim, the Xilinx

blocksets can be downloaded onto Xilinx FPGA boards. In fact, the model at this point is already an IP (Intellectual Property) Core.

5.3   Conclusion

The goal of this final year project is to design a robust synchronization algorithm for WiMAX system. The focus of the work is on the baseband inner receiver. Synchronization is aided or accelerated with the incorporation of the training symbol that helps in various estimations. The training symbol is created by modulating odd subcarriers with a PN sequence which leads to a symbol with equal halves in time domain but of opposite polarities. In this proposed algorithm, only one symbol is required as compared to two in the original Schmidl and Cox method. This effectively reduces the overhead by half. Frame timing synchronization is achieved via double sliding window packet detection. The metric that is produces will have a sharp peak in all conditions even in low SNR channels. After identifying the peak, the received samples are delayed accordingly and aligned to this index. The remaining synchronization tasks i.e. carrier frequency synchronization is accomplished using Schmidl and Cox technique. This method can accommodate frequency offsets of up to 39 062.5 Hz in a 20 MHz channel. The angle of *P(d)* is proportional to this frequency offset and has a constant value throughout the plateau of *M(d)*. Correction for the frequency offset is accomplished via multiplication of the received samples with the conjugated version of the estimated offset. With this, all synchronization tasks are complete. All in all, the proposed algorithm can achieve rapid synchronization with only one training symbol.

REFERENCES

[1] Applications for WiMAX. October 13, 2006. [Online]. Available at http://www.wimax.com/education /wimax/ims, October 30, 2006.

[2] IEEE Personal Communications, Special Issue on IMT-2000: Standards Efforts of the ITU, vol. 4, no. 4, Aug. 1997.

[3] IEEE, "*Part 16: Air Interface for Fixed Broadband Wireless Access Systems,*" IEEE Standard 802.16, 2004.

[4] WiMAX Forun, "*IEEE 802.16a Standard and WiMAX - Igniting Broadband Wireless Access White Paper,*" WiMAX Forum 2004.

[5] Wireless architectures – WiMAX. [Online]. Available at http://www.wimax.com/education/wimax/wireless_architectures, October 30, 2006.

[6] WiMAX VoIP. [Online]. Available at http://www.wimax.com/education/wimax/voip, October 30, 2006.

[7] WiMAX & IPTV. [Online]. Available at http://www.wimax.com/education/wimax/iptv, October 30, 2006.

[8] R. van Nee and R. Prasad, "*OFDM for Wireless Multimedia Communications,*" Boston: Artech House, 2000.

[9] K. Witrisal, "*OFDM Air-Interface for Multimedia Communications,*" Ph.D Thesis, Technische Universiteit Delft, Netherlands, 2002.

[10] T. M. Schmidl and D. C. Cox, "*Robust frequency and timing synchronization for OFDM,*" IEEE Trans. Commun., vol. 45, no. 12, pp. 1613–1621, Dec. 1997.

[11] Wu, J., "*Telecommunication Systems Chip Design,*" Lecture Notes, National Tsing Hua University, China.

[12] Muhammad Imadur Rahman, Suvra Sekhar Das, Frank H.P. Fitzek, "*OFDM Based WLAN Systems,*" Technical Report R-04-1002; v1.2, Center for TeleInFrastruktur (CTiF), Aalborg University, Denmark,18 February 2005.]

[13] Mattias Olsson, "*A Rapid Prototype of an IEEE802.11a Synchronizer,*" M.S. Thesis, Linkoping University, Sweden, November 13, 2002.

[14] Zhang Lili, *"A study of IEEE 802.16a OFDM-PHY Baseband,"* M.S. Thesis, Linkoping University, Sweden, February 16, 2005.

[15] Tan Jit Ken, *"An Adaptive Orthogonal Frequency Division Multiplexing Baseband Modem for Wideband Wireless Channels,"* M.S. Thesis, Massachusetts Institute of Technology, May 2006.

[16] Nicola Laurenti, *"Implementation Issues in OFDM Systems,"* Ph.D Thesis, Università degli Studi di Padova, 1998.

[17] Y. H. Kim, Y. K. Hahm, H. J. Jung, and I. Song, *"An efficient frequency offset estimator for timing and frequency synchronization in OFDM systems,"* in Proc. IEEE 1999 Pacific Rim Conf. on Commun., Computers and Signal Proc., pp. 580–583.

[18] Andrea Goldsmith, *"Wireless Communications,"* Cambridge University Press, 2006.

[19] Simon Haykin, Michael Moher, *"Modern Wireless Communication,"* Prentice-Hall, Inc., 2005.

[20] J. Bingham, *"Multicarrier modulation for data transmission: an idea whose time has come,"* IEEE Commun. Mag. Vol. 28, No. 5, pp. 5-14, May 1990.

[21] H. Sari et al., "Transmission Techniques for Digital Terrestrial TV Broadcasting," IEEE Comm. Mag., vol. 33, no. 2, pp. 100–109, February 1995.

[22] Dick, C. and Harris, F. "FPGA implementation of an OFDM PHY," Signals, Systems and Computers 2003. Conference Record of the 37th Asilomar Conference, vol. 1 pp. 905 – 909, Nov. 2003.

[23] picoChip, "WiMax : OFDM Synchronization on the picoArray," 07 April 2004.

APPENDICES

APPENDIX A

CYCLIC PREFIX – FROM LINEAR CONVOLUTION TO CYCLIC CONVOLUTION[*]

Consider a channel input sequence $x[n] = x[0], \ldots, x[N-1]$ of length N and a discrete-time channel with finite impulse response (FIR) $h[n] = h[0], \ldots, h[\mu]$ of length $\mu + 1 = T_m/T_s$, where T_m is the channel delay spread and T_s the sampling time associated with the discrete time sequence. The cyclic prefix for $x[n]$ is defined as $\{x[N-\mu], \ldots, x[N-1]\}$: it consists of the last μ values of the $x[n]$ sequence. For each input sequence of length N, these last μ samples are appended to the beginning of the sequence. This yields a new sequence $\tilde{x}[n]$, $\mu \leq n \leq N-1$, of length $N+\mu$, where $\tilde{x}[-\mu], \ldots, \tilde{x}[N-1] = x[N-\mu], \ldots, x[N-1], x[0], \ldots, x[N-1]$, as shown in Figure 12.5. Note that with this definition, $\tilde{x}[n] = x[n]_N$ for $-\mu \leq n \leq N-1$, which implies that $\tilde{x}[n-k] = x[n-k]_N$ for $-\mu \leq n-k \leq N-1$.
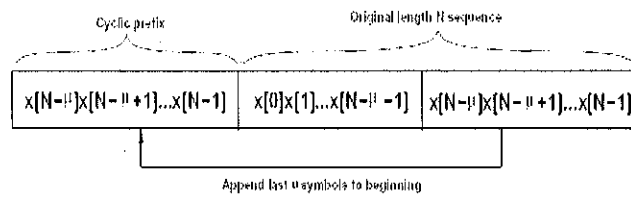

Figure 12.5: Cyclic Prefix of Length μ.

Suppose $\tilde{x}[n]$ is input to a discrete-time channel with impulse response $h[n]$. The channel output $y[n], 0 \leq n \leq N-1$ is then

$$
\begin{aligned}
y[n] &= \tilde{x}[n] * h[n] \\
&= \sum_{k=0}^{\mu-1} h[k]\tilde{x}[n-k] \\
&= \sum_{k=0}^{\mu-1} h[k]x[n-k]_N \\
&= x[n] \circledast h[n],
\end{aligned}
\tag{12.18}
$$

---

[*] Adapted from [18]

51

APPENDIX B

EQUAL HALF PROPERTY OF THE FFT

The generic IFFT is given as

$$x[n] = \frac{1}{N} \sum_{k=0}^{N-1} X(k) e^{j2\pi k/N}$$

Without a loss of generality, it can be decomposed into even and odd components

$$x[n] = \frac{1}{N} \left\{ \sum_{m=0}^{N/2-1} X(k) e^{j2\pi mn/N} + \sum_{m=0}^{N/2-1} X(k) e^{j2\pi(2m+1)n/N} \right\}$$

Where $k = 2m$ for even frequency components and $k = 2m + 1$ for odd frequency components. When modulating on even subcarriers only

$$x[n] = \frac{1}{N} \sum_{m=0}^{N/2-1} X(k) e^{j2\pi k/(N/2)}$$

The time domain signal is only $N/2$ points long. Evaluating x[n+N/2]

$$x[n + N/2] = \frac{1}{N} \sum_{m=0}^{N/2-1} X(k) e^{j2\pi(n+N/2)/N} e^{j\pi m}$$

The last exponential term evaluates to +1 when even subcarriers are modulated and -1 when odd subcarriers are modulated. Hence, this verifies that modulating odd subcarriers results in a training symbol with equal halves in time domain but opposite signs.

APPENDIX C

FREQUENCY OFFSET ESTIMATION

At optimum timing index, P(d) is as follows

$$P(d_{opt}) = \sum_{i=0}^{L-1} s_{d_{opt+i}}{}^* e^{-j(2\pi\delta f i/N+\theta)} \bullet -s_{d_{opt+i}}{}^* e^{-j(2\pi\delta f(i+L)/N+\theta)}$$

$$= -\sum_{i=0}^{L-1} \left| s_{d_{opt+i}} \right|^2 e^{-j(2\pi\delta fL)/N}$$

With this,

$$\therefore 2\pi\delta fL / N = \angle P(d_{opt})$$

$$\hat{\delta f} = \frac{1}{\pi} \angle [-P(d_{opt})]$$